
Article:
Speers, L.J., Schmidt, R. orcid.org/0000-0002-2474-3744 and Bilkey, D.K. (2022) Aberrant phase precession of lateral septal cells in a maternal immune activation model of schizophrenia risk may disrupt the integration of location with reward. Journal of Neuroscience, 42 (20). pp. 4187-4201. ISSN 0270-6474

https://doi.org/10.1523/JNEUROSCI.0039-22.2022

Aberrant phase precession of lateral septal cells in a maternal immune activation model of schizophrenia risk may disrupt the integration of location with reward

Authors

Lucinda J. Speers[1], Robert Schmidt[3], David K. Bilkey[1*]

[1]Psychology Dept., Otago Univ. Dunedin, New Zealand, [3]Psychology Dept., Univ. of Sheffield., Sheffield, United Kingdom.

Contact information: Professor David Bilkey, Department of Psychology, University of Otago, Dunedin 9054, New Zealand. Email: david.bilkey@otago.ac.nz

Number of pages: 41
Number of figures: 7
Number of words: Abstract – 249
Introduction – 655
Discussion – 1525

Declaration of interests

The authors declare no competing financial interests.

Acknowledgements

Support was provided through funding from the Health Research Council of New Zealand grant number 19/044.

Abstract

Spatial memory and reward processing are known to be disrupted in schizophrenia. Since the lateral septum (LS) may play an important role in the integration of location and reward, we examined the effect of maternal immune activation (MIA), a known schizophrenia risk factor, on spatial representation in the rat LS. In support of a previous study, we found that spatial location is represented as a phase code in the rostral LS of adult male rats, so that LS cell spiking shifts systematically against the phase of the hippocampal, theta-frequency, local field potential (LFP) as an animal moves along a track towards a reward (phase precession). Whereas shallow precession slopes were observed in control (CTL) group cells, they were steeper in the MIA animals, such that firing frequently precessed across several theta cycles as the animal moved along the length of the apparatus, with subsequent ambiguity in the phase representation of location. Furthermore, an analysis of the phase trajectories of the CTL group cells revealed that the population tended to converge towards a common firing phase as the animal approached the reward location. This suggested that phase coding in these cells might signal both reward location and the distance to reward. By comparison the degree of phase convergence in the MIA-group cells was weak, and the region of peak convergence was distal to the reward location. These findings suggest that a schizophrenia risk factor disrupts the phase-based encoding of location-reward relationships in the LS, potentially smearing reward representations across space.

Significance statement

It is unclear how spatial or contextual information generated by hippocampal cells is converted to a code that can be used to signal reward location in regions such as the ventral tegmental area. Here we provide evidence that the firing phase of cells in the LS, a region that links the two areas, may code reward location in the firing phase of cells. This phase coding is disrupted in a maternal immune activation (MIA) model of schizophrenia risk such that representations of reward may be smeared across space in MIA animals. This could potentially underlie erroneous reward processing and misattribution of salience in schizophrenia.

Previous studies suggest that the lateral septum (LS) integrates spatial and locomotor information with reward (Bender et al., 2015; Luo et al., 2011; Wirtshafter & Wilson, 2019, 2020, 2021). The primary output of hippocampal CA1 cells that signal location (O'keefe & Nadel, 1978) is to the LS (Risold & Swanson, 1997; Swanson & Cowan, 1977), and the LS in turn has reciprocal connections to several regions involved in reward processing, including the ventral tegmental area (VTA) and the striatum (Groenewegen, Vermeulen-Van der Zee, Te Kortschot, & Witter, 1987; Luo et al., 2011; Zhang, Navarrete, Wu, & Zhou, 2022). Consistent with this connectivity, the integrity of LS transmission is required for the acquisition and flexible maintenance of conditioned place preferences (Cazala, Galey, & Durkin, 1988; Jiang et al., 2018).

Recent work has shown that the LS uses both rate and phase coding to represent location (Takamura et al., 2006; Tingley & Buzsáki, 2018; Wirtshafter & Wilson, 2020; Zhou, Tamura, Kuriwaki, & Ono, 1999). For example, rate-coding cells that fire when an animal is in a specific region of space, known as the cell's "place field" have been observed in more dorsal regions of LS, although these place fields are not as robust as those observed in the hippocampus (Takamura et al., 2006; Wirtshafter & Wilson, 2020). However, in more rostral regions of the LS, cells display little evidence of rate coding but appear to encode spatial location via phase precession (Tingley & Buzsáki, 2018).

Phase precession refers the observation that, as an animal moves through space, the temporal spiking of principal cells systematically advances relative to the background theta oscillation (O'Keefe & Recce, 1993; Skaggs, McNaughton, Wilson, & Barnes, 1996). When phase precession occurs in an assembly of cells it produces theta sequences (Foster & Wilson, 2007), thereby allowing for the sequential order of experience to be reproduced within a compressed timescale that is suitable for synaptic plasticity (Dan & Poo, 2004). It has been proposed that these phenomena underlie the sequential ordering of information that

86 evolves across time and space (Buzsáki & Tingley, 2018), and that they may play an
87 important role in learning and memory processes (Dragoi & Buzsáki, 2006; Jaramillo &
88 Kempter, 2017). These proposals have been supported by a growing body of work (Feng,
89 Silva, & Foster, 2015; Gupta, Van Der Meer, Touretzky, & Redish, 2012; Terada, Sakurai,
90 Nakahara, & Fujisawa, 2017; Wang et al., 2015; Wikenheiser & Redish, 2015), and recent
91 evidence has described phase precession and theta sequences in humans (Heusser, Poeppel,
92 Ezzyat, & Davachi, 2016; Qasim, Fried, & Jacobs, 2020).
93 Neurodevelopmental abnormalities and dysfunctional activity have been observed in
94 the septum of individuals with schizophrenia, including abnormal spiking activity and LFP
95 oscillations (Heath & Peacock, 2013; Heath & Walker, 1985). Furthermore, changes in LS
96 activity have been observed in both in vivo and in vitro studies following administration of
97 either antipsychotic or dissociative drugs in animal models (Contreras, Dorantes, Mexicano,
98 & Guzmán-Flores, 1986; Sheehan, Chambers, & Russell, 2004; Yu et al., 2002). The spatial
99 and contextual memory deficits (Brébion, David, Pilowsky, & Jones, 2004; Fajnerová et al.,
100 2014; Glahn et al., 2003; Hanlon et al., 2006; Park & Holzman, 1992; Rizzo et al., 1996;
101 Salgado-Pineda et al., 2016; Waters, Maybery, Badcock, & Michie, 2004; Weniger & Irle,
102 2008) and abnormal reward processing (Jensen et al., 2008; Strauss, Waltz, & Gold, 2013;
103 Whitton, Treadway, & Pizzagalli, 2015) that have been observed in schizophrenia may
104 therefore be linked to LS dysfunction.
105 In the present study we investigated whether a risk factor for schizophrenia,
106 maternal immune activation (MIA) altered LS activity. The MIA model is based on robust
107 epidemiological evidence that maternal infection during pregnancy increases the risk of
108 schizophrenia in the offspring (Adams, Kendell, Hare, & Munk-Jørgensen, 1993; Brown &
109 Meyer, 2018). When this is modelled in rodents, MIA animals have many schizophrenia-like

behavioral, cognitive and neural deficits (Bitanihirwe et al., 2010; Savanthrapadian et al., 2013; Wolff, Cheyne, & Bilkey, 2011).

Materials and methods

ANIMALS AND EXPERIMENTAL DESIGN

All subjects were generated using the MIA intervention described previously by Dickerson, Wolff, and Bilkey (2010), Wolff and Bilkey (2015) and Speers et al. (2021). Female Sprague Dawley rats (~3 months old) were time-mated with GD1 considered to be the first day after copulation. On GD 15, pregnant dams were anesthetized with isoflurane (5%; Bayer) and administered either a single injection of polyinosinic:polycytidylic acid (poly I:C; Sigma-Aldrich) 4.0 mg/kg, i.v. dissolved in 0.9% saline (Baxter), or an equivalent saline injection 1 ml/kg. This dosage is the most common induction protocol used for rats (Haddad, Patel, & Schmid, 2020). A number of previous studies have examined the precise timing of injections on developmental phenotypes, with injections performed around GD 15 in rats leading to more robust phenotypes associated with schizophrenia than earlier injection protocols, which have been associated more with autism spectrum disorders (Haddad et al., 2020). Poly I:C and saline treatments were always performed in pairs.

Due to resource limitations, all litters were culled to a maximum of 6 male pups and were housed in open cages prior to weaning. Post-weaning, male offspring were randomly allocated a litter number and then housed in littermate groups of 2-3 in individually ventilated cages (IVC). CTL and MIA animals were housed in a single housing room, which was maintained at a normal 12-h light/dark cycle, and temperature controlled to 20-22ºC. Juvenile rats were provided with access to food *ad libitum*, and after 3 months were food deprived to no less than 85% of their free-feeding weight in preparation for the experimental procedure.

Water was available *ad libitum* throughout the entire experimental procedure. All rats weighed between 400 and 650g at the time of surgery.

APPARATUS AND TRAINING

Animals ran in a rectangular circuit measuring 900 by 800mm (Figure 1a). All arms were 100mm wide with 270mm high side walls and constructed of wood. The entire apparatus was painted in matte black and was devoid of visual cues. A video camera was mounted on the ceiling of the recording room to view the whole apparatus. All experiments were performed in a darkened environment with some ambient light from the recording computer and a small lamp aimed away from the apparatus into one corner of the room.

The experimental procedure was identical to the procedure described previously in Speers et al. (2021). Adult male offspring were randomly selected according to their litter number, with a maximum of two animals per litter, and were trained over a period of 5 to 15 days. On days 1-5 rats were habituated to the recording room, apparatus and food reward, and were allowed to free-forage for Coco Pops (Kellogg Company) scattered throughout the apparatus. Following successful habituation, whereby rats actively explored the maze and consumed the food reward, the placement of Coco Pops was gradually restricted, first to the top 2 corners of the track and the centre of the reward arm, and then to the reward arm only. During this period, rats were trained to run in a clockwise direction and were turned back to the correct direction with a barrier when necessary. Coco-pops (approx. 6 per reward delivery) were delivered manually by the experimenter. Training was considered completed when rats consistently ran in a clockwise direction for the food reward over a twenty-minute session.

SURGICAL PROCEDURES

All experimental protocols were approved by the Otago University Animal Ethics Committee and conducted in accordance with New Zealand animal welfare legislation. Following successful training, animals were anesthetized with 5% isoflurane (Merial New Zealand) in oxygen and maintained at 1.5 to 2.5% throughout surgery. After animals were anesthetized, they were given a subcutaneous injection of Atropine (1mg/kg) to ease their breathing, as well as the analgesics Carprofen (1mg/kg) and Temgesic (buprenorphine; 0.1mL), and a prophylactic antibiotic, Amphoprim (trimethoprim and sulfamethazine, 0.2mL). Rats were then mounted on a stereotaxic apparatus (David Kopf Instruments) above a heating pad, and a lubricating eye gel (Visine) was applied. The scalp was shaved and sterilized with Betadine (Povidone-iodine), followed by a subcutaneous injection in the scalp of the local anesthetic Lopaine (lignocaine hydrochloride 20mg mL^{-1}; 0.1mL diluted in 0.4mL of saline). After exposing the skull, two openings were drilled above the left hemisphere, one above the dorsal CA1 region of the hippocampus, and one above the septal region. A custom built, 8 channel, adjustable microdrive containing 1 tetrode and 1 tritrode bundle of equal length was implanted at +.5mm AP, -1.5mm ML, and was lowered to ~ 4mm from dura at an angle of ~7-8 degrees towards the midline (Figure 1b. Tetrodes consisted of 25µm nichrome, heavy formvar insulated wire (Stablohm 675 HFV NATRL; California Fine Wire Company), and had been gold electroplated until impedances were reduced to ~ 200 – 300 kΩ (NanoZ, Neuralynx). A non-movable LFP electrode was separately implanted in CA1 at -3.8mm AP from bregma and -2.5mm ML from the midline, and then lowered to 2mm from dura (Figure 1c). Microdrives were secured to the skull with jewellers' screws and dental cement, and a ground wire was secured to an additional screw placed above the right hemisphere. Post-surgery rats received a secondary dose of Amphoprim immediately upon waking, and then an additional dose of Carprofen 24 hours later. Rats were provided with ad libitum food and water post-surgery and were given 8 days to recover.

EXPERIMENTAL PROCEDURE AND ELECTROPHYSIOLOGICAL RECORDINGS

Following recovery, rats were again food deprived to no less than 85% of their free-feeding weight. Post-operative training and test trials were carried out in the recording room. Rats were attached to a multichannel data acquisition system (DacqUSB; Axona Ltd), and single unit data was closely monitored during test trials, which consisted of a 5-10 minute recording session. Extracellular unit activity was first passed through an AC-coupled unity gain amplifier before passing through to the recording system. Single unit data was bandpass filtered between 600 and 6000 Hz, and sampled at a rate of 48 kHz with 24-bit resolution. For each tetrode, one electrode with minimal spiking activity was selected as a reference. Action potential thresholds were set at a minimum of 70 – 80 μV and recorded for a 1 ms window whenever the spiking amplitude was above this threshold. All spike events were time-stamped relative to the beginning of the recording. LFP data was simultaneously recorded from the CA1 region, was bandpass filtered up to 500 Hz (with notch filtering selective for activity at 50 Hz) with a gain of ~500, and sampled at 48 kHz. The animal's location was determined from 3 infrared LEDs mounted on the animal's head-stage and recorded by a camera located above the chamber. Positional data was analysed with a sampling rate of 50 Hz and then converted into x and y coordinates by the recording system.

During the test period, tetrodes were slowly lowered (~40μm per day) until well-isolated single units were identified. Once single unit activity was confirmed, tetrodes were lowered an additional ~40μm after every second recording for the remainder of the experimental procedure. Experimental recordings were 20 minutes long, and testing continued for ~3-8 weeks, until there was no further evidence of single unit activity, manual adjustment had reached its limit, or the rat experienced other difficulties that terminated the

experiment. Final electrode placements are shown in Figures 1e and 1f. Rats ran no more than one session per day, for ~60 – 80 laps per session. Single unit, position and LFP data was saved for later analysis. All recordings with at least 1 putative place cell were included in the final dataset.

ISOLATION OF SINGLE UNITS

For each recording, single units were identified manually offline using purpose designed cluster cutting software (Plexon Offline Sorter, Version 3), primarily via the peak-to-valley distance and principal components analysis of the waveforms. All stable waveforms with clearly observed spike clustering were included in the initial analysis, regardless of spike-width or firing rate. Example waveforms and cluster cutting from both CTL and MIA recordings are presented in Figures 1d. Sorted data was then exported to MATLAB (version R2019a, MathWorks), and analysis of single unit, position and LFP data was carried out in MATLAB with custom-written scripts.

SELECTION OF FIRING ONSET LOCATION AND PHASE PRECESSION ANALYSIS

Initial inspection of firing properties around the track indicated that, although some cells only fired in a portion of the track, the majority of cells fired indiscriminately across the entire track. Where it did occur, the onset location of firing also appeared to vary from cell to cell, and could appear at any point along the track. Due to this variability and lack of clear place fields, manual selection of firing starting location and termination was used for phase precession analysis. To these ends all cell recordings were split into groups of ~20 cells and assigned a blinded identifier to ensure experimenter bias was minimized during the manual selection process. These blind groups were then analysed with a custom MATLAB script that first linearized the track, and then allowed the experimenter to select the start and end

234 locations of firing across 2 cycles of the track. For cells that only fired across a portion of the
235 track, firing onset and offset locations were always selected as the locations where robust
236 firing began and ended in a clockwise direction respectively. For cells that fired
237 indiscriminately across the entire track, the start location was selected on the basis of the
238 following criteria, in order: 1) a small pause in the firing, 2) the location where clear phase
239 precession could be observed to begin relative to random noise, and 3, if no clear firing
240 pauses or phase precession relative to noise were observed, then the analysis region was
241 always started just after the reward location, and ended just before the reward location.
242
243 DATA ANALYSIS
244 LFP activity recorded from electrode located in CA1 was sampled at 4800Hz. To
245 determine theta waveform shape, the LFP was bandpass filtered between 6-10Hz and a phase
246 profile was determined using the Hilbert transform. A sample waveform of 200 ms duration
247 was subsequently captured whenever the phase data indicated a trough had been reached.
248 These samples were then averaged, as were the related phase profiles.
249 Spatial information values, a measure of how informative a spike from a cell is
250 regarding the animal's current location within an environment, were calculated according to
251 the method described in Skaggs, McNaughton, and Gothard (1993). The formula for
252 information content, measured in bits per spike is:

$$Information = \sum_{i=1}^{N} p_i \frac{\lambda_i}{\lambda} log2 \frac{\lambda_i}{\lambda}$$

253 where the environment is divided into N distinct bins ($i = 1, \ldots, N$), p_I denotes the
254 occupancy probability of bin i, λ_i is the mean firing rate for bin i, and λ is the overall mean
255 firing rate of the cell. Higher information values indicate that cells provide a more reliable
256 prediction of current location than cells with lower information values.

Correlations of hippocampal theta frequency and speed were generated for each recording that showed evidence of single unit activity in the LS. This process involved estimating instantaneous values for theta frequency from the Hilbert transform of LFP filtered between 6 and 10 Hz. Estimates of instantaneous speed were determined by monitoring the animals change in position over 500 ms time windows. Speed and theta frequency data were then sampled at one second intervals and correlated. Samples where speed was below 5 cm/s were excluded from the analysis.

For all phase precession analyses, the phase reference was always to the LFP signal recorded from the non-movable electrode implanted in CA1, where a phase of zero corresponded to the trough of the oscillation. Phase precession was determined by matching the animal's position to the instantaneous phase of the 6-10 Hz theta rhythm at the CA1 reference, as determined from the Hilbert transform. These data were then analysed using procedures described previously (Kempter et al., 2012; Speers et al., 2021). This involves using circular-linear regression to provide a robust estimate of the slope and phase offset of the regression line, and a correlation coefficient for circular-linear data analogous to the Pearson product-moment correlation coefficient for linear-linear data. Phase precession analysis was conducted by pooling spiking data from all passes through the region of interest within a given recording session. The number of phase cycles per track was calculated as the absolute value of the slope (in degrees per mm) multiplied by the length of the full track, and then divided by 360. LS phase precession as described by Tingley and Buzsáki (2018) would generally produce a value of around 1.

Correlations of firing rate and either speed or acceleration were based on the process outlined by Wirtshafter and Wilson (2019). For this analysis, position was sampled every 100 ms to estimate instantaneous speed. These data were then smoothed across a 500 ms window. The animals' occupancy per speed within 2cm/s bins was then established and then

spike count as a function of speed was determined. Spike count per speed was then divided by speed occupancy to result in firing rate as a function of speed for each cell of interest. Speeds with less than 2% of total occupancy were excluded from the analysis. The correlation between speed and firing rate was assessed using a linear regression. Correlations with acceleration were determined similarly except that a bin size of 0.5 cm/s^2 was used.

To allow between-animal comparison of phase trajectories across the track it was first necessary that any phase shift that might have resulted from variation in the depth of the hippocampal electrode was minimised. To this end the phase relationship between theta activity recorded at the moveable LS electrode was compared to that recorded at the fixed hippocampal electrode using cross correlation of LFP data filtered between 6-10Hz. It was determined that phase shifted systematically as the LS electrode was lowered, but for some animals this phase/depth relationship was offset at equivalent LS electrode depths. This indicated that the depth of the reference hippocampal electrode was different between animals, as theta phase varies depending on electrode position above and below the CA1 cell layer (Brankačk, Stewart, & Fox, 1993; Buzsáki, Rappelsberger, & Kellényi, 1985; Lubenov & Siapas, 2009). With this information theta-frequency LFP phase difference between the two electrodes was normalised to zero when LS electrodes were 4.5 mm deep from the dura (see Figure 6b). All normalised phase trajectories were projected both forward and backwards across the full extent of the linearized track. To determine whether there was any tendency for phase trajectories to intersect at a particular location along the track, the phase angle of each phase trajectory was determined in one cm increments along the track. A population vector was then calculated for each location for all intercepting phase trajectories. The subsequent population vector could vary from zero, indicating no clustering of phase trajectories at this location, to one, which would indicate that all phase trajectories intersected at one phase angle at that location.

To determine whether LS cells tended to fire in bursts at near-theta frequencies, an autocorrelation of cell spiking with a +/-500 ms window was conducted across each recording. The dominant frequency between 6 and 10 Hz was determined from the power spectrum of the autocorrelation function.

HISTOLOGY

Following completion of experiments, animals were anaesthetised with 5% isoflurane in oxygen, and a 2mA direct current was passed through each electrode for approximately 1 second to lesion the site of the electrode tip. Rats were then euthanized with an overdose of isoflurane and transcardially perfused, first with 120 ml of 0.9% saline, and then 120 ml of 10% formalin in saline. Brains were then carefully extracted from the skull after removal of the Microdrive, and stored in 10 % formalin in saline. One week prior to sectioning, brains were transferred first to 10% formalin in H_2O for 24 hours, and then to a 10% formalin/30% sucrose solution for approximately 3-7 days, until the brain sunk to the bottom of the sucrose solution. Dehydrated brains were then sectioned into 60 μm coronal slices with a cryostat (Leica CM1950). Sections were then mounted on slides and stained with a thionine acetate Nissl stain (Santa Cruz Biotechnology, Inc. After slides were dry (min. 24 hours) electrode placement was imaged with a local power (1.5x) digital microscope (Leica Biosystems, LLC) to verify electrode placement (Figures 1e and 1f).

STATISTICAL ANALYSES

For all statistical analyses, we performed the following procedure. First, raw data was transformed to a lognormal distribution if appropriate. All data (either in raw form or the log transform) were then checked for assumptions of normality. These checks were performed in GraphPad Prism 8.1.1 (GraphPad Software, Inc., San Diego, CA, USA), using the d'Agostino

& Pearson test for normality. If data did not meet the assumptions for normality based on the d'Agostino & Pearson test, visual inspection of histograms and QQ plots was performed, and extreme outliers were removed using the Graphpad function for removal of outliers. All data that failed to meet assumptions of normality based on this procedure were then analysed using the appropriate non-parametric test. Details about the specific tests used are provided in the results section. All t-tests were two-tailed. Data with a normal distribution are presented as mean ± SEM unless explicitly stated otherwise in the figure legends. For all data that did not meet normality assumptions, the median with 95% confidence intervals is depicted instead. Significance levels were defined as $p < 0.05$. Additional information about significance levels is provided in the figures as: * $p < 0.05$, ** $p < 0.01$, *** $p < 0.001$. Additional circular statistics (to compare group differences in the intercept of the circular correlation of phase and position, and to generate the MVL for animal by animal and litter by litter analyses) were performed in Oriana 4 (Kovach Computing Services, Inc., Anglesey, UK). Group differences for angular variance (defined as 1-MVL) were performed using the variance ratio F-test, found at https://www.statskingdom.com/220VarF2.html

Results

Tetrode verification in the rostral LS

Single units were recorded from eight animals (7 litters) in both the CTL and MIA groups respectively. However, one CTL animal was later excluded from further analyses due to electrode misplacement in the medial septum (figure 1e). This decision was made not only based on tetrode placement close to the MS, but also following inspection of other firing properties suggesting that cells recorded from this animal were atypical. For example, cells recorded from this animal had a significantly higher firing rate when compared to the average firing rate of all other cells (figure 1e, lover right corner), and inspection of phase precession

plots showed that these cells were tightly coupled to specific phases of the LFP theta rhythm, consistent with the firing properties of GABAergic medial septal neurons (Borhegyi et al., 2004). After excluding this animal, a total of 144 units from seven CTL animals (6 litters) and 362 units from eight MIA (7 litters) were used for all subsequent analyses. All animals were age matched except for one pair, in which the CTL animal was seven months and the corresponding MIA animal was twelve months, and one non-paired MIA animal (12 months). All ages refer to animal age during experimental recordings, and ranged from 4 to 14 months. There was no difference in the mean ages between groups (CTL = 10.43 ± 1.49, MIA = 11.25 ± 1.13, $t(13) = 0.45$, $p = 0.664$).

Basic firing properties of LS cells, mean locomotor speed, and comparison of hippocampal theta properties

The median firing rate for all LS cells was 0.44 Hz, 95% CI [0.35, 0.51]. The median log transformed firing rate was significantly higher for cells in the MIA group (-0.25, 95% CI [-0.34, -0.11] than in the CTL group (-0.71, 95% CI [-0.80, -0.59], Mann Whitney U =16638, $p < 0.001$; Figure 2a). Visual inspection of the distribution of firing rates around the track indicated that activity was distributed relatively diffusely across the track for both groups. In support of this observation, the spatial information content measure for all cells was low (median = 0.69 bits/spike, 95% CI [0.59, 0.77]). It was, however, significantly lower for cells in the MIA group (median = 0.59, 95% CI [0.51, 0.71] compared to cells in the CTL group (median = 0.82, 95% CI [0.71, 0.96], Mann Whitney U = 22555, $p = 0.007$; Figure 2b). In a further quantification of spatial firing we identified the subset of cells where the contiguous region of firing (as selected by the firing onset and offset locations) was less than half the track length (<150cm), and where the spatial information content was greater than 0.8 bits/spike (Wirtshafter & Wilson, 2019). Only 4.7 and 5.8% of cells in the CTL and MIA

groups respectively met these criteria, confirming that spatially selective activity was rare for both groups. There was no significant difference in these proportions between groups ($\chi^2(1) = 0.54$, $p = 0.46$).

The mean theta-frequency LFP amplitude recorded from electrodes located in the CA1 region were significantly higher in the CTL group (M (log-transformed) = 3.17 ± 0.03, MIA M = 3.07 ± 0.02, $t(286) = 2.66$, $p = 0.008$; Figure 2d). The mean frequency of theta-band CTL LFP recordings (M= 7.92 Hz ± 0.02) was also significantly higher than in MIA recordings (M = 7.72 Hz ± 0.02, $t(286) = 7.0$, $p < 0.001$; Figure 2f), although the phase profile was virtually identical for both groups (Figure 2h).

Mean running speed was significantly lower in the MIA group (29.61 cm/s ± 0.50) than for the CTL group (M=31.42 cm/s ± 0.57, $t(279) = 2.35$, $p = 0.02$; Figure 2c). To determine whether this affected the theta-locomotion relationship (Bender et al., 2015) we sampled hippocampal theta frequency and speed values once every second and computed the correlation between these values for each individual recording. A comparison of the resultant r values revealed that the median r value was slightly lower in the CTL group (median = 0.35, 95% CI [0.30,0.39]) when compared to the MIA group (median = 0.39, 95% CI [0.34, 0.24], but the difference was not significantly different (Mann Whitney U = 8482, $p = 0.059$), although only marginally. There were no significant differences for either the slope of these correlations (CTL M = 6.97 ± 0.38, MIA M = 7.36 ± 0.31, $t(284) = 0.80$, $p = 0.426$), or the intercept (CTL M = -37.12 ± 3.02, MIA M = -39.86 ± 2.49, $t(284) = 0.7$, $p = 0.485$).

LS cells in the MIA group continue to demonstrate robust phase precession, but are more likely to precess through multiple theta cycles across the running track

In total 34.03% of all cells in the CTL group and 30.12 % of all cells in the MIA group showed evidence of significant phase precession (Figure 4a). This difference was not

statistically significant (χ^2 (1) = 0.74. p = 0.391). Examples are provided in Figure 3a (CTL) and 3b (MIA). The circular-linear correlation of phase and position, as calculated across all cells, was significantly higher in the CTL group (median = -0.07, 95% CI [-0.08, -0.05], MIA median = -0.03, 95% CI [-0.04,-0.02], Mann-Whitney U = 21292, p = 0.001), although the p-values of those correlations were not different between groups (CTL median = 0.162, 95% CI [0.109, 0.269], MIA median = .244, 95% CI [0.191, 0.313], Mann Whitney U = 25017, p = 0.481). The same analyses were then performed on the subset of cells showing significant phase precession. The difference between the circular-linear correlations for this subset was non-significant although the result was marginal (CTL mean r = -0.14 ± 0.02, MIA mean r = -0.10 ± 0.01, t (156) = 1.94, p = 0.054; Figure 4b). A similar, marginal result was obtained for the p-value of the circular-linear correlation (CTL median = 0.004, 95% CI [0.001, 0.012], MIA median = 0.001, 95% CI [<0.001, 0.003], Mann Whitney U = 2155, p = 0.052; Figure 4c).

Visual comparison of phase precession trajectories across the track indicated that many cells in the MIA group precessed through several theta cycles over the circuit (Figure 3b). By comparison this firing behaviour was observed in few cells from the CTL group. Furthermore, when firing in MIA animals was analysed on a pass by pass basis, there were a number of examples where firing cycled through more than 360 degrees, indicating that the multiple-cycle precession was not simply a cumulative effect produced by variation on individual passes (Schmidt et al., 2009). Analysis of the slope values obtained from the circular-linear fit from all cells revealed that MIA group cells had a significantly steeper slope when compared to CTL group cells (CTL median = -352 deg/mm, 95% CI [-435.7, -188.3], MIA median = -522.2 deg/mm, 95% CI [-623.2, -468.1], Mann Whitney U = 20158, p <0.001; Figure 4d, left side). A similar result was obtained for the subset of cells demonstrating significant phase precession (CTL median = -173.8 deg/mm, 95% CI [-351, -

122], MIA median = -526.4 deg/mm, 95% CI [-700, -424.9], Mann Whitney U = 1536, p <0.001; Figure 4d, right side). The length of track over which these slope values were calculated was not significantly different between groups (CTL median = 2662mm, 95% CI [2523, 2871], MIA median = 2585mm, 95% CI [2468, 2815], Mann Whitney U = 2523, p = 0.581). By combining these slope values and the length of the track over which they were calculated, it was possible to determine the number of phase precession cycles that would occur across the entire track length, were precession to continue across the whole region. For cells that demonstrated significant phase precession, the median number of phase precession cycles in the CTL group was 0.79. This was significantly lower than the median number of cycles in the MIA group (1.89 cycles, Mann Whitney U = 1562, p <0.001; Figure 4e).

To confirm that these slope differences were not a result of aberrant recordings from a small proportion of MIA animals, mean values were also computed for each individual animal and then compared across groups. For this analysis, only cells that demonstrated significant phase precession were analysed. Comparison of slope values on an animal by animal basis showed that MIA slope values were significantly steeper than CTL slope values (CTL mean = -325.6 deg/mm ± 50.28, MIA mean = -534.2 deg/mm ± 69.81, t(13) = 2.36, p = 0.035; Figure 4f).

Dual oscillator theories of phase precession suggest that a change in the slope of precession in MIA animals might result from an alteration in the theta-frequency/cell-burst-firing-frequency relationship (Kamondi, Acsády, Wang, & Buzsáki, 1998; Magee, 2001; Mehta, Lee, & Wilson, 2002; O'Keefe & Recce, 1993). To test this hypothesis, the burst firing frequency of single cells was calculated. For both MIA and CTL groups mean burst firing frequency was slightly higher than theta frequency, but there was no significant difference in cell-burst frequency between the two groups (CTL median = 8.3 Hz, 95% CI [8.06, 8.55], MIA median = 8.06 Hz, 95% CI [8.06, 8.06], Mann Whitney U 11452, p =

0.658; Figure 4h). As described previously, theta frequency was significantly lower in MIA animals. As an approximation of how this difference might affect precession, for controls the theta/burst relationship would result in cell firing precessing through a full 360 degrees in approximately three seconds. In contrast, in MIA animals this precession would occur in around 2.3 seconds. Thus, based on this difference MIA would precess around 30% faster than control animals. This contrasts with the actual difference in precession cycles around the track, which is closer to a 2-fold difference between MIA and controls (figure 4e).

Starting phase is more variable for MIA cells when compared to CTL cells

To determine the phase of cell firing as an animal enters the analysis region, the intercept of the regression line for the circular linear-correlation was examined. Only cells that demonstrated significant phase precession were included in this analysis. LS cells in both the CTL and MIA groups demonstrated significant clustering at a mean phase angle of 314.83º (CTL Raleigh $Z = 15.78$, $p < 0.001$) and 288.96º (MIA Raleigh $Z = 12.36$, $p < 0.001$), around the starting phase. The circular variance of starting phase for MIA group cells was, however, significantly greater than for CTL group cells (CTL = 0.43, MIA = 0.66, $F = 0.43$, $p = 0.001$; Figure 4i). The Mardia-Watson Wheeler test, which considers group differences in both the mean and variance for circular data, also returned a significant result ($W = 8.99$, $p = 0.011$). As a further test, the circular distance from the mean angle was computed for each cell and then compared across groups. Again, MIA group cells had a significantly higher median distance from the mean angle when compared to CTL group cells (Mann Whitney $U = 1996$, $p = 0.011$), indicating that precession starting phase was more variable in the MIA group.

Lead/lag times between the hippocampus and LS vary systematically according to electrode depth

Previous studies indicate that the firing phase of LS cells changes systematically according to electrode depth (Tingley & Buzsáki, 2018). To examine this possibility, a lead/lag analysis was performed for each recording to determine the phase shift of LS LFPs when referenced to the non-movable hippocampal electrode. These results were then correlated with LS electrode depth on an animal by animal basis (figure 5a). In the majority of animals, the LS was more likely to lead the hippocampus at shallow depths, but as electrode depth increased, the hippocampus was more likely to lead the LS. However, this relationship was not always observed in the MIA group, with 3 animals showing the opposite relationship. A t-test of the regression slopes of the depth/phase relationship indicated that mean slopes were more positive in the CTL group ($M = 35.37 \pm 6.0$ when compared to the MIA group ($M = 8.82 \pm 9.72$, $t(13) – 2.24$, $p = 0.043$). Inspection of the individual animal phase and LS electrode depth relationship suggested that a number of animals (across both groups) had greater hippocampal lead relative to depth (figure 5a). This was most likely due to variability in hippocampal electrode depth (Brankačk et al., 1993; Buzsáki et al., 1985; Lubenov & Siapas, 2009). To correct for this in further analyses, the phase of all recordings was shifted, on a whole-animal basis, to align with a reference where zero phase shift occurred at an electrode depth of 4500 microns (figure 5b).

Relationship between firing phase and reward location

In prior analyses LS cell phase precession had been examined across sections of the track where firing occurred. As a result, data from different cells was often from different (although often overlapping) regions of the track. To examine how the phase trajectories of individual cells (the best fit to the firing phase-position data) would appear if precession was

assumed to continue from the start of the linearized track to the end, these phase trajectories were normalized for differences in lead/lag likely resulting from variation in hippocampal electrode position as described above, and then extended in each direction so as to cover the whole track (Figures 5c and f). Inspection of these plots for CTL group cells indicated that a large number of these individual phase trajectories tended to intersect near the location on the track where the reward was delivered. To quantify this effect, each trajectory was allocated a phase angle at each location on the track, based on the phase of firing at this location. Then for each location on the track the average phase angle and mean vector length (MVL) across the whole population of trajectories was determined. This procedure was repeated at one cm increments along the whole track. The MVL thus provided a measure of the degree of intersection of the phase trajectories at each location, which could vary from zero, indicating no clustering of phase trajectories at that location, to one, which would indicate that all phase trajectories intersected at that location. These resultant data indicated that CTL group MVL was highest (0.50) at the reward location (Figure 5d). At the location with the highest MVL, CTL group phase angles were significantly clustered with a mean phase angle of 200.06º (Rayleigh $Z = 11.78$, $p < 0.001$; Figure 6e). When the same analysis was applied to the MIA data, phase trajectories were overall less convergent (maximum MVL=0.24) with greatest convergence occurring well prior to the reward location (Figure 5g). At the reward location there was little evidence of convergence in MIA trajectories (MVL = 0.08; mean angle of 236.29º, Raleigh $Z = 0.699$, $p = 0.497$; Figure 5h). A Mardia-Watson-Wheeler test revealed significantly greater clustering at the reward location in the CTL compared to the MIA groups (MWW= 12.92, $p = 0.002$).

Firing rates of a substantial subset of cells located in the rostral LS are significantly correlated with speed for both groups, but positive correlations were significantly more frequent in the MIA group

Recent work has demonstrated that the dorsal LS contains a population of cells for which firing rate has a strong linear relationship with either speed or acceleration (Howe & Blair, 2020; Wirtshafter & Wilson, 2019). To examine whether cells located in the rostral LS are also modulated by speed, we computed Pearson correlations of speed and firing rate for each cell (example correlations are provided in Figure 6a. In total, just over 30% of all CTL group cells had firing rates that were significantly correlated with speed, in contrast to almost 45% of all MIA group cells. These proportions were significantly different ($\chi^2(1) = 8.6$, $p = 0.003$. From these significant subsets, 45% of all cells in the CTL group and 59% of cells in the MIA group had firing that was positively correlated with speed (Figure 6b). Again, these proportions were significantly different between groups ($\chi^2(2) = 10.61$, $p = 0.005$). When the absolute median r-values generated by these correlations were compared across the entire dataset, they were also significantly higher in the MIA group (CTL median = 0.41, 95% CI [0.31, 0.51], MIA median = 0.56, 95% CI [0.51, 0.60], Mann Whitney U = 20426, $p < 0.001$: Figure 6c). The median r-values were also compared separately according to the direction of these correlations for those data where significant correlations between firing rate and speed were observed. Results from this reduced data subset showed that there were no group differences for the median r-values for either positive correlations (CTL median = 0.77, 95% CI [0.69, 0.88], MIA median = 0.81, 95% CI [0.78, 0.85], Mann Whitney U = 861, $p = 0.517$) or negative correlations (CTL median = -0.75, 95% CI [-0.80, -0.70], MIA median = -0.79, 95% CI [-0.81, -0.74], Mann Whitney U = 674, $p = 0.245$, Figure 6c).

To test the possibility that spatial and locomotor information map onto distinct cell populations, the group of cells demonstrating significant phase precession ("phase coding

554 cells") was compared with the group of cells that had firing rates significantly correlated with
555 speed ("speed modulated cells") to determine if there was any overlap. Of the 49 phase
556 coding cells in the CTL group, 18 were also speed modulated cells, including 12 cells with a
557 positive speed correlation. In total, only 24% of all CTL group cells that had either phase
558 coding or speed modulated properties were involved in both these processes simultaneously.
559 In the MIA group, 59 out of 109 phase coding cells were also classed as speed modulated
560 cells, including 43 cells with positive speed correlations (Figure 6d). In total, this amounted
561 to 28% of cells with overlapping coding properties. These proportions were not significantly
562 different between groups ($\chi^2(1) = 0.41$, $p = 0.52$).

563 The firing of a relatively small proportion of cells were modulated by the animal's
564 acceleration. In total 8% of CTL group cells and 9% of MIA group cells displaying a
565 significant correlation with either acceleration or deceleration (Figure 6e). These proportions
566 were not significantly different between groups ($\chi^2(2) = 1.57$, $p = 0.456$). The difference
567 between the absolute r-values were also not significant for either acceleration (CTL median =
568 0.25, 95% CI [0.17, 0.29], MIA median = 0.24, 95% CI [0.19, 0.28], Mann Whitney U =
569 14400, $p = 0.657$) or deceleration (CTL median = 0.23, 95% CI [0.21, 0.27], MIA median =
570 0.22, 95% CI [0.20, 0.26], Mann Whitney U = 24385, $p = 0.673$; Figure 6e), and similar
571 results were obtained when only those cells with significant correlations were included in the
572 analysis (for acceleration, CTL $M = 0.67 \pm 0.03$, MIA $M = 0.74 \pm 0.05$, $t(18) = 1.07$, $p =$
573 0.299; for deceleration, CTL $M = 0.64 \pm 0.05$, MIA $M = 0.66 \pm 0.04$, $t(20) = 0.21$, $p = 0.834$).
574

575 **Discussion**

576 We investigated whether MIA altered neuronal coding of location in the rostral LS, a
577 region which is likely to provide an important link between location coding mechanisms and
578 reward systems (Bender et al., 2015; Luo et al., 2011; Wirtshafter & Wilson, 2019, 2020,

2021). Most cells fired indiscriminately across the majority of the track, with only a small proportion of cells (~5%) in both the CTL and MIA groups showing evidence of spatially selective firing reminiscent of place cells. This is consistent with previous reports that sampled cells from the rostral LS (Tingley & Buzsáki, 2018) and contrasts with prior studies targeting the dorsal LS, where LS "place fields" (Wirtshafter & Wilson, 2020) (Takamura et al., 2006) have been described. These data therefore provide corroborating evidence that the rate coding of location varies across LS sub-regions.

Approximately a third of all LS cells displayed evidence of significant phase coding of location across both groups. This is considerably less than the 89% of cells reported to display phase coding in the Tingley and Buzsáki (2018) study. It should be noted, however, that they used different criteria to determine whether cells showed evidence of phase coding, and our methodology is likely more conservative. During phase coding in CTL cells the phase of firing typically precessed across a single theta cycle as animals navigated the full length of the track (Tingley & Buzsáki, 2018). In contrast, although the MIA manipulation did not compromise the ability of LS cells to precess, there was a significantly steeper slope of precession. In many cells, this resulted in phase precession that circulated through several 360-degree cycles as the animal traversed the track. Phase precession in excess of a single theta cycle has not generally been observed in previous studies of the phenomenon (Dragoi & Buzsáki, 2006; Ekstrom, Meltzer, McNaughton, & Barnes, 2001; Geisler et al., 2007; Huxter, Burgess, & O'Keefe, 2003; Kamondi et al., 1998; Kjelstrup et al., 2008; Maurer et al., 2006; O'Keefe & Recce, 1993; Royer, Sirota, Patel, & Buzsáki, 2010; Schmidt et al., 2009; Skaggs et al., 1996; Terrazas et al., 2005; Tingley & Buzsáki, 2018). Instead, phase range has been shown to dynamically shift according to either place field size or route familiarity across a range of experimental paradigms so that that precession remains restricted to 360 degrees across a place field (Ekstrom et al., 2001; Kjelstrup et al., 2008; Royer et al., 2010; Terrazas

et al., 2005). It is possible that the multiple phase precession cycles observed in the MIA group represent more discrete "place fields" that are entirely decoupled from firing rate, with discrete "fields" anchored to salient features of the animal's current environment or specific task demands (Gupta et al., 2012; Maurer et al., 2006). In contrast, CTL animals may be more likely to collate these discrete environmental "chunks" into a coherent whole as the animal becomes more familiar with a learned navigational route (see figure 7).

When CTL phase trajectories were projected across the full length of the track, as a population they tended to converge so that LS cells were firing at around the peak of theta activity as recorded at the CA1 cell layer. This convergence was maximal at the location of reward delivery. In contrast there was no evidence of phase trajectory convergence at the reward region in MIA animals. The one previous paper that has described and examined phase coding in the LS concluded that the LS phase code was likely agnostic to reward location, however, this analysis was not a major focus of the paper, and some neurons were clearly linked to local cues such as the goal (Tingley & Buzsáki, 2018). Our finding contributes to a growing body of evidence indicating that the LS is involved in the integration of spatial and reward information (Bender et al., 2015; Luo et al., 2011; Wirtshafter & Wilson, 2019, 2020, 2021), and similar to phase precession in the ventral striatum, suggests that firing phase in the LS may contain information about reward proximity or salience (van der Meer & Redish, 2011). It should be noted, however, that we did not systematically manipulate reward location in our study, to isolate it from other local cues. Further study would be required to test this hypothesis.

If phase of firing signals reward location and distance to reward then we would predict that in the MIA animals the association between reward and location is 'smeared' across the environment such that a far broader range of stimuli and locations become associated with the reward. Since the LS has direct connections to the VTA, this effect may

model, and potentially provide a mechanism for, some of the changes observed in schizophrenia (Zhang et al., 2022). In particular altered motivational salience (Kapur, 2003), which occurs with dysregulated dopamine signals and a tendency for individuals to mis-assign salience to the elements of experience.

One of the most salient landmarks available to animals in this study was the presence of corners and it is interesting to note that the limited phase trajectory convergence that occurred in MIA animals may have been tied to the corners of the apparatus (see figure 5g). Corners not only provide sensory information, but they require bidirectional modifications of locomotor activity to navigate around them. Approximately one third of cells had significant correlations of firing rate and speed, which is about half the figure reported by Wirtshafter and Wilson (2019), but substantially more than that reported by Tingley and Buzsáki (2018). The proportion of CTL group cells with firing rates that were negatively correlated with speed was also just over half of all significantly correlated cells, in contrast to only around one third in the Wirtshafter and Wilson (2019) study, suggesting that cells located in the rostral LS may be particularly important for monitoring speed during tasks that involve bidirectional speed fluctuations. Animals may have been able to move at a more constant speed in the Tingley and Buzsáki (2018) due to the circular running apparatus.

A previous study from our lab showed that MIA disrupts theta sequences in the CA1 region of the hippocampus (Speers et al., 2021). According to predictions of the dynamic weighting model proposed by Tingley and Buzsáki (2018), disrupted CA1 theta sequences should prevent LS phase precession. However, in the current study, the proportion of cells showing evidence of significant phase precession was not statistically different between groups. Taken together, these data suggest that the MIA manipulation did not compromise the ability of LS to precess relative to the CA1 theta oscillation, suggesting that upstream disruptions of phase coding in the hippocampus do not abolish phase coding in the LS. They

may, however, interfere with how spatial information is discretized relative to reward locations. Additional studies will be required, however, to test whether the MIA-induced changes in LS phase precession are a direct result of disrupted theta sequences in the hippocampus, or are reflective of some other change.

It is unclear what mechanism(s) might account for the steeper phase precession observed in MIA animals. Our results showed that hippocampal theta frequency was significantly slower in MIA animals, while at the same time the intrinsic burst frequency of cells did not differ between groups, consistent with a 'detuned oscillator' (Drieu & Zugaro, 2019) explanation of the increase in phase precession slope. The magnitude of change predicted by this model, did not, however, fully explain our observations. Alternatively, according to somato-dendritic interference models (Drieu & Zugaro, 2019), an increase in the rate of excitatory ramping onto LS neurons might produce the same effect, although this ramping would have to be cyclic across the apparatus to produce the effect observed and would fail to produce precession of greater than 180 degrees on a single pass.

These results provide further evidence that phase coding may be disturbed following MIA (Speers et al., 2021), and suggest a biophysical mechanism for impaired integration of contextual and reward information, which may explain why MIA animals display memory impairments when multi-sensory integration is required (Ballendine et al., 2015; Howland, Cazakoff, & Zhang, 2012). Impaired spatial-reward integration could also have profound downstream effects on motivation and dopamine signalling, both of which are known to be impaired in schizophrenia (Davis, Kahn, Ko, & Davidson, 1991; Strauss et al., 2013). Consistent with this idea, a recent study has demonstrated that dysregulation of the CA1-LS pathway induces both dopaminergic hyperactivity in the VTA and novelty-induced hyper-locomotion that is schizophrenia-like, and that these could be attenuated via inhibition of the LS (Zhang et al., 2022). The apparent smearing of reward representations across space, and

potentially time, by LS cells is also likely to compromise the development of conditioned place preferences (Cazala et al., 1988; Jiang et al., 2018; Regier et al., 1990). It may also underlie MIA-induced changes in reward and temporal processing (Deane, Millar, Bilkey, & Ward, 2017; Millar, Bilkey, & Ward, 2017). The abnormal discretization of spatial representations could also contribute to the impaired attentional filtering and aberrant salience that have been described in schizophrenia (Kapur, 2003; Luck, Leonard, Hahn, & Gold, 2019), and also in autism spectrum disorder (Bodner, Cowan, & Christ, 2019), another MIA-associated neurodevelopmental disorder. (Haddad et al., 2020).

Adams, W., Kendell, R., Hare, E., & Munk-Jørgensen, P. (1993). Epidemiological evidence that maternal influenza contributes to the aetiology of schizophrenia: An analysis of Scottish, English, and Danish data. *The British Journal of Psychiatry, 163*(4), 522-534.

Ballendine, S. A., Greba, Q., Dawicki, W., Zhang, X., Gordon, J. R., & Howland, J. G. (2015). Behavioral alterations in rat offspring following maternal immune activation and ELR-CXC chemokine receptor antagonism during pregnancy: implications for neurodevelopmental psychiatric disorders. *Progress in Neuro-Psychopharmacology and Biological Psychiatry, 57*, 155-165.

Bender, F., Gorbati, M., Cadavieco, M. C., Denisova, N., Gao, X., Holman, C., Korotkova, T., & Ponomarenko, A. (2015). Theta oscillations regulate the speed of locomotion via a hippocampus to lateral septum pathway. *Nature communications, 6*(1), 1-11.

Bitanihirwe, B. K., Peleg-Raibstein, D., Mouttet, F., Feldon, J., & Meyer, U. (2010). Late prenatal immune activation in mice leads to behavioral and neurochemical abnormalities relevant to the negative symptoms of schizophrenia. *Neuropsychopharmacology, 35*(12), 2462.

Bodner, K. E., Cowan, N., & Christ, S. E. (2019). Contributions of filtering and attentional allocation to working memory performance in individuals with autism spectrum disorder. *Journal of abnormal psychology, 128*(8), 881.

Borhegyi, Z., Varga, V., Szilágyi, N., Fabo, D., & Freund, T. F. (2004). Phase segregation of medial septal GABAergic neurons during hippocampal theta activity. *Journal of Neuroscience, 24*(39), 8470-8479.

Brankačk, J., Stewart, M., & Fox, S. E. (1993). Current source density analysis of the hippocampal theta rhythm: associated sustained potentials and candidate synaptic generators. *Brain research, 615*(2), 310-327.

Brébion, G., David, A. S., Pilowsky, L. S., & Jones, H. (2004). Recognition of visual stimuli and memory for spatial context in schizophrenic patients and healthy volunteers. *Journal of Clinical and Experimental Neuropsychology, 26*(8), 1093-1102.

Brown, A. S., & Meyer, U. (2018). Maternal immune activation and neuropsychiatric illness: a translational research perspective. *American Journal of Psychiatry, 175*(11), 1073-1083.

Buzsáki, G., Rappelsberger, P., & Kellényi, L. (1985). Depth profiles of hippocampal rhythmic slow activity ('theta rhythm') depend on behaviour. *Electroencephalography and clinical neurophysiology, 61*(1), 77-88.

Buzsáki, G., & Tingley, D. (2018). Space and time: The hippocampus as a sequence generator. *Trends in cognitive sciences, 22*(10), 853-869.

Cazala, P., Galey, D., & Durkin, T. (1988). Electrical self-stimulation in the medial and lateral septum as compared to the lateral hypothalamus: differential intervention of reward and learning processes? *Physiology & behavior, 44*(1), 53-59.

Contreras, C. M., Dorantes, M. E., Mexicano, G., & Guzmán-Flores, C. (1986). Lateralization of spike and wave complexes produced by hallucinogenic compounds in the cat. *Experimental neurology, 92*(3), 467-478.

Dan, Y., & Poo, M.-m. (2004). Spike timing-dependent plasticity of neural circuits. *Neuron, 44*(1), 23-30.

Davis, K. L., Kahn, R. S., Ko, G., & Davidson, M. (1991). Dopamine in schizophrenia: a review and reconceptualization. *The American journal of psychiatry*.

Deane, A. R., Millar, J., Bilkey, D. K., & Ward, R. D. (2017). Maternal immune activation in rats produces temporal perception impairments in adult offspring analogous to those observed in schizophrenia. *PloS one, 12*(11), e0187719.

744 Dickerson, D. D., Wolff, A. R., & Bilkey, D. K. (2010). Abnormal long-range neural
745 synchrony in a maternal immune activation animal model of schizophrenia. *Journal of*
746 *Neuroscience, 30*(37), 12424-12431.
747 Dragoi, G., & Buzsáki, G. (2006). Temporal encoding of place sequences by hippocampal
748 cell assemblies. *Neuron, 50*(1), 145-157.
749 Drieu, C., & Zugaro, M. (2019). Hippocampal Sequences During Exploration: Mechanisms
750 and Functions. *Frontiers in Cellular Neuroscience, 13*, 232.
751 Ekstrom, A., Meltzer, J., McNaughton, B., & Barnes, C. (2001). NMDA receptor antagonism
752 blocks experience-dependent expansion of hippocampal "place fields". *Neuron, 31*(4),
753 631-638.
754 Fajnerová, I., Rodriguez, M., Levčík, D., Konrádová, L., Mikoláš, P., Brom, C., Stuchlík, A.,
755 Vlček, K., & Horáček, J. (2014). A virtual reality task based on animal research–
756 spatial learning and memory in patients after the first episode of schizophrenia.
757 *Frontiers in behavioral neuroscience, 8*, 157.
758 Feng, T., Silva, D., & Foster, D. J. (2015). Dissociation between the Experience-Dependent
759 Development of Hippocampal Theta Sequences and Single-Trial Phase Precession.
760 *Journal of Neuroscience, 35*(12), 4890-4902. doi:10.1523/Jneurosci.2614-14.2015
761 Foster, D. J., & Wilson, M. A. (2007). Hippocampal theta sequences. *Hippocampus, 17*(11),
762 1093-1099.
763 Geisler, C., Robbe, D., Zugaro, M., Sirota, A., & Buzsáki, G. (2007). Hippocampal place cell
764 assemblies are speed-controlled oscillators. *Proceedings of the National Academy of*
765 *Sciences, 104*(19), 8149-8154.
766 Glahn, D. C., Therman, S., Manninen, M., Huttunen, M., Kaprio, J., Lönnqvist, J., & Cannon,
767 T. D. (2003). Spatial working memory as an endophenotype for schizophrenia.
768 *Biological psychiatry, 53*(7), 624-626.
769 Groenewegen, H., Vermeulen-Van der Zee, E. t., Te Kortschot, A., & Witter, M. (1987).
770 Organization of the projections from the subiculum to the ventral striatum in the rat.
771 A study using anterograde transport of Phaseolus vulgaris leucoagglutinin.
772 *Neuroscience, 23*(1), 103-120.
773 Gupta, A. S., Van Der Meer, M. A., Touretzky, D. S., & Redish, A. D. (2012). Segmentation
774 of spatial experience by hippocampal theta sequences. *Nature neuroscience, 15*(7),
775 1032.
776 Haddad, F., Patel, S., & Schmid, S. (2020). Maternal immune activation by Poly I: C as a
777 preclinical model for neurodevelopmental disorders: a focus on autism and
778 schizophrenia. *Neuroscience & Biobehavioral Reviews*.
779 Hanlon, F. M., Weisend, M. P., Hamilton, D. A., Jones, A. P., Thoma, R. J., Huang, M.,
780 Martin, K., Yeo, R. A., Miller, G. A., & Cañive, J. M. (2006). Impairment on the
781 hippocampal-dependent virtual Morris water task in schizophrenia. *Schizophrenia*
782 *research, 87*(1-3), 67-80.
783 Heath, R. G., & Peacock, J. (2013). ADDENDUM E. ELECTROENCEPHALOGRAMS
784 AND SUBCORTICOGRAMS RECORDED SINCE THE JUNE 1952 MEETINGS.
785 In *Studies in Schizophrenia* (pp. 573-608): Harvard University Press.
786 Heath, R. G., & Walker, C. F. (1985). Correlation of deep and surface electroencephalograms
787 with psychosis and hallucinations in schizophrenics: a report of two cases. *Biological*
788 *psychiatry*.
789 Heusser, A. C., Poeppel, D., Ezzyat, Y., & Davachi, L. (2016). Episodic sequence memory is
790 supported by a theta–gamma phase code. *Nature neuroscience, 19*(10), 1374.
791 Howe, A. G., & Blair, H. T. (2020). Excitatory and inhibitory modulation of septal and
792 striatal neurons during hippocampal sharp-wave ripple events. *bioRxiv*.

Howland, J., Cazakoff, B., & Zhang, Y. (2012). Altered object-in-place recognition memory, prepulse inhibition, and locomotor activity in the offspring of rats exposed to a viral mimetic during pregnancy. *Neuroscience, 201*, 184-198.

Huxter, J., Burgess, N., & O'Keefe, J. (2003). Independent rate and temporal coding in hippocampal pyramidal cells. *Nature, 425*(6960), 828-832.

Jaramillo, J., & Kempter, R. (2017). Phase precession: a neural code underlying episodic memory? *Current opinion in neurobiology, 43*, 130-138.

Jensen, J., Willeit, M., Zipursky, R. B., Savina, I., Smith, A. J., Menon, M., Crawley, A. P., & Kapur, S. (2008). The formation of abnormal associations in schizophrenia: neural and behavioral evidence. *Neuropsychopharmacology, 33*(3), 473.

Jiang, J. X., Liu, H., Huang, Z. Z., Cui, Y., Zhang, X. Q., Zhang, X. L., Cui, Y., & Xin, W. J. (2018). The role of CA3-LS-VTA loop in the formation of conditioned place preference induced by context-associated reward memory for morphine. *Addiction biology, 23*(1), 41-54.

Kamondi, A., Acsády, L., Wang, X. J., & Buzsáki, G. (1998). Theta oscillations in somata and dendrites of hippocampal pyramidal cells in vivo: Activity-dependent phase-precession of action potentials. *Hippocampus, 8*(3), 244-261.

Kapur, S. (2003). Psychosis as a state of aberrant salience: a framework linking biology, phenomenology, and pharmacology in schizophrenia. *American Journal of Psychiatry, 160*(1), 13-23.

Kempter, R., Leibold, C., Buzsáki, G., Diba, K., & Schmidt, R. (2012). Quantifying circular–linear associations: Hippocampal phase precession. *Journal of neuroscience methods, 207*(1), 113-124.

Kjelstrup, K. B., Solstad, T., Brun, V. H., Hafting, T., Leutgeb, S., Witter, M. P., Moser, E. I., & Moser, M.-B. (2008). Finite scale of spatial representation in the hippocampus. *Science, 321*(5885), 140-143.

Lubenov, E. V., & Siapas, A. G. (2009). Hippocampal theta oscillations are travelling waves. *Nature, 459*(7246), 534.

Luck, S. J., Leonard, C. J., Hahn, B., & Gold, J. M. (2019). Is Attentional Filtering Impaired in Schizophrenia? *Schizophrenia bulletin, 45*(5), 1001-1011.

Luo, A. H., Tahsili-Fahadan, P., Wise, R. A., Lupica, C. R., & Aston-Jones, G. (2011). Linking context with reward: a functional circuit from hippocampal CA3 to ventral tegmental area. *Science, 333*(6040), 353-357.

Magee, J. C. (2001). Dendritic mechanisms of phase precession in hippocampal CA1 pyramidal neurons. *Journal of neurophysiology, 86*(1), 528-532.

Maurer, A. P., Cowen, S. L., Burke, S. N., Barnes, C. A., & McNaughton, B. L. (2006). Organization of hippocampal cell assemblies based on theta phase precession. *Hippocampus, 16*(9), 785-794.

Mehta, M., Lee, A., & Wilson, M. (2002). Role of experience and oscillations in transforming a rate code into a temporal code. *Nature, 417*(6890), 741.

Millar, J., Bilkey, D. K., & Ward, R. D. (2017). Maternal immune activation alters sensitivity to action-outcome contingency in adult rat offspring. *Brain, behavior, and immunity, 63*, 81-87.

O'keefe, J., & Nadel, L. (1978). *The hippocampus as a cognitive map*: Oxford: Clarendon Press.

O'Keefe, J., & Recce, M. L. (1993). Phase relationship between hippocampal place units and the EEG theta rhythm. *Hippocampus, 3*(3), 317-330.

Park, S., & Holzman, P. S. (1992). Schizophrenics show spatial working memory deficits. *Archives of general psychiatry, 49*(12), 975-982.

842 Paxinos, G., & Watson, C. (2006). *The rat brain in stereotaxic coordinates: hard cover*
843 *edition*: Elsevier.
844 Qasim, S. E., Fried, I., & Jacobs, J. (2020). Phase precession in the human hippocampus and
845 entorhinal cortex. *bioRxiv*.
846 Regier, D. A., Farmer, M. E., Rae, D. S., Locke, B. Z., Keith, S. J., Judd, L. L., & Goodwin,
847 F. K. (1990). Comorbidity of mental disorders with alcohol and other drug abuse:
848 results from the Epidemiologic Catchment Area (ECA) study. *Jama, 264*(19), 2511-
849 2518.
850 Risold, P., & Swanson, L. (1997). Connections of the rat lateral septal complex. *Brain*
851 *Research Reviews, 24*(2-3), 115-195.
852 Rizzo, L., Danion, J.-M., Van Der Linden, M., Grangé, D., & Rohmer, J.-G. (1996).
853 Impairment of memory for spatial context in schizophrenia. *Neuropsychology, 10*(3),
854 376.
855 Royer, S., Sirota, A., Patel, J., & Buzsáki, G. (2010). Distinct representations and theta
856 dynamics in dorsal and ventral hippocampus. *Journal of Neuroscience, 30*(5), 1777-
857 1787.
858 Salgado-Pineda, P., Landin-Romero, R., Portillo, F., Bosque, C., Pomes, A., Spanlang, B.,
859 Franquelo, J. C., Teixido, C., Sarró, S., & Salvador, R. (2016). Examining
860 hippocampal function in schizophrenia using a virtual reality spatial navigation task.
861 *Schizophrenia research, 172*(1-3), 86-93.
862 Savanthrapadian, S., Wolff, A. R., Logan, B. J., Eckert, M. J., Bilkey, D. K., & Abraham, W.
863 C. (2013). Enhanced hippocampal neuronal excitability and LTP persistence
864 associated with reduced behavioral flexibility in the maternal immune activation
865 model of schizophrenia. *Hippocampus, 23*(12), 1395-1409.
866 Schmidt, R., Diba, K., Leibold, C., Schmitz, D., Buzsáki, G., & Kempter, R. (2009). Single-
867 trial phase precession in the hippocampus. *Journal of Neuroscience, 29*(42), 13232-
868 13241.
869 Sheehan, T. P., Chambers, R. A., & Russell, D. S. (2004). Regulation of affect by the lateral
870 septum: implications for neuropsychiatry. *Brain Research Reviews, 46*(1), 71-117.
871 Skaggs, W. E., McNaughton, B. L., & Gothard, K. M. (1993). *An information-theoretic*
872 *approach to deciphering the hippocampal code.* Paper presented at the Advances in
873 neural information processing systems.
874 Skaggs, W. E., McNaughton, B. L., Wilson, M. A., & Barnes, C. A. (1996). Theta phase
875 precession in hippocampal neuronal populations and the compression of temporal
876 sequences. *Hippocampus, 6*(2), 149-172.
877 Speers, L. J., Cheyne, K. R., Cavani, E., Hayward, T., Schmidt, R., & Bilkey, D. K. (2021).
878 Hippocampal sequencing mechanisms are disrupted in a maternal immune activation
879 model of schizophrenia risk. *The Journal of Neuroscience*, JN-RM-0730-0721.
880 doi:10.1523/jneurosci.0730-21.2021
881 Strauss, G. P., Waltz, J. A., & Gold, J. M. (2013). A review of reward processing and
882 motivational impairment in schizophrenia. *Schizophrenia bulletin, 40*(Suppl_2),
883 S107-S116.
884 Swanson, L., & Cowan, W. (1977). An autoradiographic study of the organization of the
885 efferet connections of the hippocampal formation in the rat. *Journal of Comparative*
886 *Neurology, 172*(1), 49-84.
887 Takamura, Y., Tamura, R., Zhou, T. L., Kobayashi, T., Tran, A. H., Eifuku, S., & Ono, T.
888 (2006). Spatial firing properties of lateral septal neurons. *Hippocampus, 16*(8), 635-
889 644.
890 Terada, S., Sakurai, Y., Nakahara, H., & Fujisawa, S. (2017). Temporal and rate coding for
891 discrete event sequences in the hippocampus. *Neuron, 94*(6), 1248-1262. e1244.

892 Terrazas, A., Krause, M., Lipa, P., Gothard, K. M., Barnes, C. A., & McNaughton, B. L.
893 (2005). Self-motion and the hippocampal spatial metric. *Journal of Neuroscience,*
894 *25*(35), 8085-8096.
895 Tingley, D., & Buzsáki, G. (2018). Transformation of a Spatial Map across the Hippocampal-
896 Lateral Septal Circuit. *Neuron*.
897 van der Meer, M. A., & Redish, A. D. (2011). Theta phase precession in rat ventral striatum
898 links place and reward information. *Journal of Neuroscience, 31*(8), 2843-2854.
899 Wang, Y., Romani, S., Lustig, B., Leonardo, A., & Pastalkova, E. (2015). Theta sequences
900 are essential for internally generated hippocampal firing fields. *Nature neuroscience,*
901 *18*(2), 282.
902 Waters, F. A., Maybery, M. T., Badcock, J. C., & Michie, P. T. (2004). Context memory and
903 binding in schizophrenia. *Schizophrenia research, 68*(2-3), 119-125.
904 Weniger, G., & Irle, E. (2008). Allocentric memory impaired and egocentric memory intact
905 as assessed by virtual reality in recent-onset schizophrenia. *Schizophrenia research,*
906 *101*(1-3), 201-209.
907 Whitton, A. E., Treadway, M. T., & Pizzagalli, D. A. (2015). Reward processing dysfunction
908 in major depression, bipolar disorder and schizophrenia. *Current opinion in*
909 *psychiatry, 28*(1), 7.
910 Wikenheiser, A. M., & Redish, A. D. (2015). Hippocampal theta sequences reflect current
911 goals. *Nature neuroscience, 18*(2), 289.
912 Wirtshafter, H. S., & Wilson, M. A. (2019). Locomotor and hippocampal processing
913 converge in the lateral septum. *Current Biology, 29*(19), 3177-3192. e3173.
914 Wirtshafter, H. S., & Wilson, M. A. (2020). Differences in reward biased spatial
915 representations in the lateral septum and hippocampus. *Elife, 9*, e55252.
916 Wirtshafter, H. S., & Wilson, M. A. (2021). Lateral Septum as a Nexus for Mood,
917 Motivation, and Movement. *Neuroscience & Biobehavioral Reviews*.
918 Wolff, A. R., & Bilkey, D. K. (2015). Prenatal immune activation alters hippocampal place
919 cell firing characteristics in adult animals. *Brain, behavior, and immunity, 48*, 232-
920 243.
921 Wolff, A. R., Cheyne, K. R., & Bilkey, D. K. (2011). Behavioural deficits associated with
922 maternal immune activation in the rat model of schizophrenia. *Behavioural brain*
923 *research, 225*(1), 382-387.
924 Yu, B., Wang, C., Liu, J., Johnson, K., & Gallagher, J. (2002). Adaptation to chronic PCP
925 results in hyperfunctional NMDA and hypofunctional GABAA synaptic receptors.
926 *Neuroscience, 113*(1), 1-10.
927 Zhang, J., Navarrete, M., Wu, Y., & Zhou, Y. (2022). 14-3-3 Dysfunction in Dorsal
928 Hippocampus CA1 (dCA1) Induces Psychomotor Behavior via a dCA1-Lateral
929 Septum-Ventral Tegmental Area Pathway. *Frontiers in Molecular Neuroscience, 15*.
930 Zhou, T. L., Tamura, R., Kuriwaki, J., & Ono, T. (1999). Comparison of medial and lateral
931 septal neuron activity during performance of spatial tasks in rats. *Hippocampus, 9*(3),
932 220-234.
933
934
935

Figure 1. Methodological details and verification of electrode placement. (a) Diagram of the rectangular track. Rats were pre-trained to run in a clockwise direction for a food reward delivered at the centre of the bottom arm (marked with the red X). (b) Tetrode placement in the LS (highlighted in yellow). The tetrodes bundles are depicted by the thick black line. Dashed purple lines indicate the initial depth of electrode placement during surgery, while red lines show the range of target location through the rostral LS over the course of the experiment. (c) Diagram of the hippocampus showing the target area for LFP surgical implantation, and an example photograph of histology demonstrating electrode placement in the pyramidal cell layer of CA1. (d) Cluster cutting examples for CTL cells (shown in blue) and MIA (yellow). These examples show some of the different spike widths and inter-spike interval histogram profiles observed in the LS. The top CTL example is similar to a canonical place field, while the second CTL cell has a similar waveform, but the histogram profile shows a more continuous spiking pattern across time. The first MIA example shows a cell with a narrower waveform and a delayed spiking profile, whereas the final example shows a broader waveform, similar to a hippocampal place cell, but the spiking profile is more reminiscent of an interneuron. These spiking profiles were common across both groups, and were chosen to demonstrate the range of different spiking profiles observed rather than systematic group differences. (e) Schematic of final tetrode location in the LS for CTL animals at the termination of the experiment. Modified stereotaxic image taken from Paxinos and Watson (2006). Percentages refer to the proportion of phase coding cells calculated individually for each animal, with phase coding cells defined as cells with a significant (<.05) circular-linear correlation of phase and position. Faded red areas delineate regions where less than 20% of all recorded cells demonstrated evidence of significant phase precession, and faded yellow delineates regions where proportions fell between 21 and 40%. Example images of tetrode placement in the rostral LS is shown below. The second example shows the final electrode placement of the excluded cell in the MS (marked with a cross). Additional inspection of firing rates of the excluded cell compared to all other cells demonstrated that they were atypical (below right). (f) As for e, but for MIA cells.

Figure 2. Basic firing properties of LS cells, mean locomotor speed, and comparison of hippocampal theta properties. (a) Median firing rate of LS cells across the entire track. (b) Information content of LS cells, measured in bits/spike. Bar denotes median values. (c) Mean locomotor speed as animals traversed the rectangular track. Bars denote mean and SEM. (d) EEG amplitude of CA1 LFP recordings. Error bars denote mean and SEM. (e) Examples of filtered and raw EEG recordings for both groups. (f) Violin plots of theta frequency in Hz. (g) Average wave form shape of CA1 LFP oscillations in the theta band. Lighter colour denotes standard error. (h) Average phase profile of the theta waveform, from the Hilbert transform. (i) Comparison of median r values for the theta frequency/ speed correlations generated for each individual recording.

Figure 3. Comparison of LS phase precession between CTL and MIA animals. (a) Example plots of phase precession in CTL cells. These examples were chosen to demonstrate a range of phase precession (PP) variability, and each example cell is taken from a different animal. For each example cell, the figure on the left displays PP as a function of colour around the track, with dark blue representative of 0º and red representative of 360º. On the right are the corresponding PP plots after linearization of the track for selected segments. Red lines denote the regression slope. In all plots, phase is repeated across 2 cycles for clarity. In the CTL group, example cell 1 demonstrates both spatially selective firing around half of the track in addition to robust PP. Example cell 2 demonstrates robust phase precession across the majority of the track, with PP around 1 full cycle. Example cell 3 demonstrates robust PP through the reward area. Example cell 4 demonstrates a shallow PP slope and sparse firing outside the reward area. (b) As for (a), but for example MIA cells. Example cell 1 demonstrates robust PP that approaches a full cycle. Example cell 2 demonstrates robust PP across the entire track, in which PP appears to reset at the top left-hand corner. Example cell 3 demonstrates robust PP through multiple cycles across the track. Example cell 4 demonstrates robust PP that precesses through 2 distinct cycles.

Figure 4. LS cells in the MIA group are more likely to precess across multiple theta cycles. (a) Proportion of LS cells with statistically significant ($p < .05$) phase precession for each group. (b) Mean r values of the circular correlation of phase and position for both groups. Error bars denote SEM. (c) p values of the circular linear correlation shown in (b). (d) Slope values (deg/mm) for all cells (on right), and for a subset of cells demonstrating significant phase precession (on left). Black lines denote median values. (e) Phase cycles across the full track. Error bars denote median with 95% confidence intervals. (f) Mean slope values of the circular-linear correlation on an animal by animal basis. Error bars denote SEM. (g) Log transformed firing rates of the subset of cells demonstrating significant phase precession. Error bars denote mean and SEM. (h) Theta burst frequency of single units. (i) Circular histograms of intercept values for both groups, demonstrating greater variability of phase precession starting phase in the MIA group. Between group differences are based on the variance ratio F test. Red bars denote the mean angle with 95% confidence intervals.

Figure 5. Relationship between firing phase and reward. (a) Correlations of LS electrode depth and lead/lag of LFPs recorded simultaneously from CA1 and the LS. Each animal is shown in a different color. Negative values indicate that the LS is leading CA1, and positive values indicate that CA1 is leading the LS. (b) Example of phase correction shift. (c) Phase trajectories of each precessing LS CTL group cell (as in figure 3a). Each trajectory is plotted onto one diagram where x-axis is linearized track. Vertical lines indicate corners and triangle marks reward location. Note how many tracks seem to pass through phase/location point at around 180º phase at the reward location. (d) Clustering of phase trajectories in the CTL group (from data in c), measured as mean vector length (MVL; y-axis), across the track (x-axis). Mean vector length can vary from 0 – no clustering to 1 - tight clustering or focus. Note that control trajectories show greatest clustering (phase focus) at the reward location (triangle). (e) Circular histogram of corrected phase angle (as shown in shown in c) when measured at the reward location. (f) Phase trajectory of each MIA group cell (as in figure 3b). Note that there is no clear clustering of phase trajectories around the reward location. (g) As in d, but for the MIA group. In contrast to the CTL group, MIA trajectories show much less clustering, with very little clustering at the reward location and less differentiation across the track. (h) As for e, but for MIA phase angles.

Figure 6. Evidence of speed modulated cells in the rostral LS. (a) Example plots demonstrating robust correlations of firing rate and speed for both groups (first 3 examples in each row). The final example in each row shows firing rates that were correlated with acceleration rather than speed. These examples were chosen to demonstrate both positive and negative correlations that were typically observed across both groups. (b) Proportion of cells with significant correlations of firing rate and speed. Significance level for the linear correlation was set at 0.05. Sig. + refers to significant positive correlations and sig. - refers to negative correlations. (c) Violin plots of the absolute r value of the firing rate/speed correlation for the entire dataset (left column). Median r values for the linear correlation of firing rate and speed when only those cells with a significant firing rate/speed correlation were included are shown on the right. Error bars include 95% confidence intervals (d) As for (b), but including cells with significant phase precession to demonstrate overlapping cell properties. (e) As for c, but for acceleration (+) and deceleration (-). Error bars denote mean and SEM.

Figure 7. Schematic of LS phase precession in CTL and MIA animals. In the CTL diagram, phase of LS cell firing (PP; coded by colour) occurs across a single cycle as the animal traverses a familiar route to a reward. In the upper rectangle, the range of PP from the starting location (S) is determined by a salient external cue marking the end of the route (white square) while other external cues (grey squares) and the reward itself (grey star) do not affect PP range. Alternatively in the lower example, PP range is anchored to the reward (white R) itself, while external cues are irrelevant. In both cases, intact theta sequences(A-D) arriving from CA1 (and potentially CA3) are likely to contribute to the emergence of single cycle PP in the LS and phase-coded information about the likelihood of rewards across the trajectory could be transmitted to subcortical regions such as the VTA. In the MIA example, disordered theta sequences from CA1 (and potentially CA3) may contribute to PP in the LS that exceeds a single theta cycle as the animal traverses a familiar route. The range of PP may be anchored to several salient cues across the trajectory (white squares), providing a more discretized representation of a navigational route in comparison to CTL animals. Alternatively, multiple cycle PP in MIA animals may reflect erroneous reward expectancies as the animal traverses the route. As a result, information about incorrect reward expectancies (red arrows) may be transmitted to the VTA, which could contribute to abnormal dopamine signalling in subcortical regions.

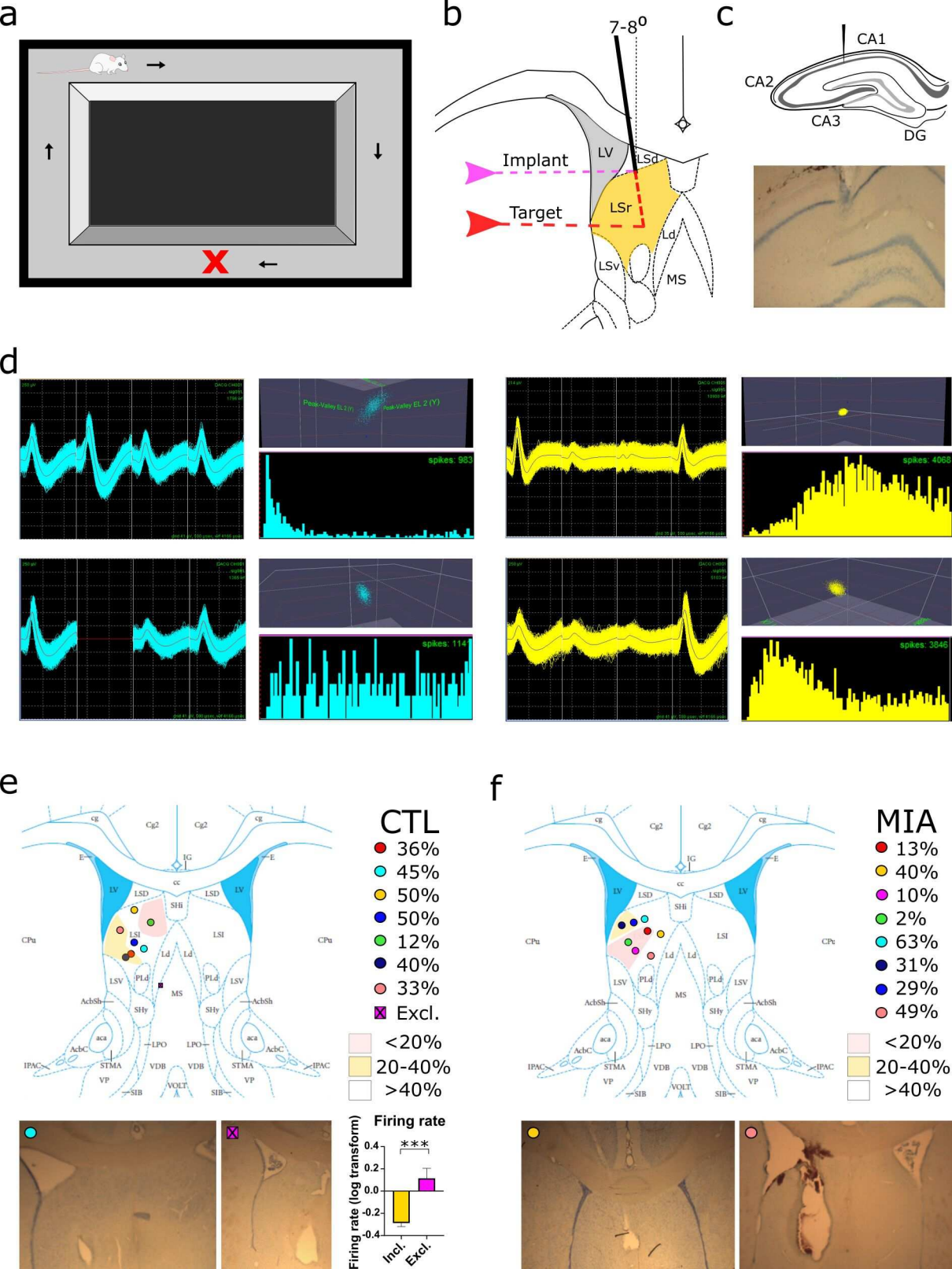
a
b
7-8°
Implant
Target
LV
LSd
LSr
Ld
LSv
MS
c
CA1
CA2
CA3
DG
d
spikes: 983
spikes: 4066
spikes: 1147
spikes: 3846
e
CTL
36%
45%
50%
50%
12%
40%
33%
Excl.
<20%
20-40%
>40%
Firing rate
***
Firing rate (log transform)
0.4
0.2
0.0
-0.2
-0.4
Incl.
Excl.
f
MIA
13%
40%
10%
2%
63%
31%
29%
49%
<20%
20-40%
>40%

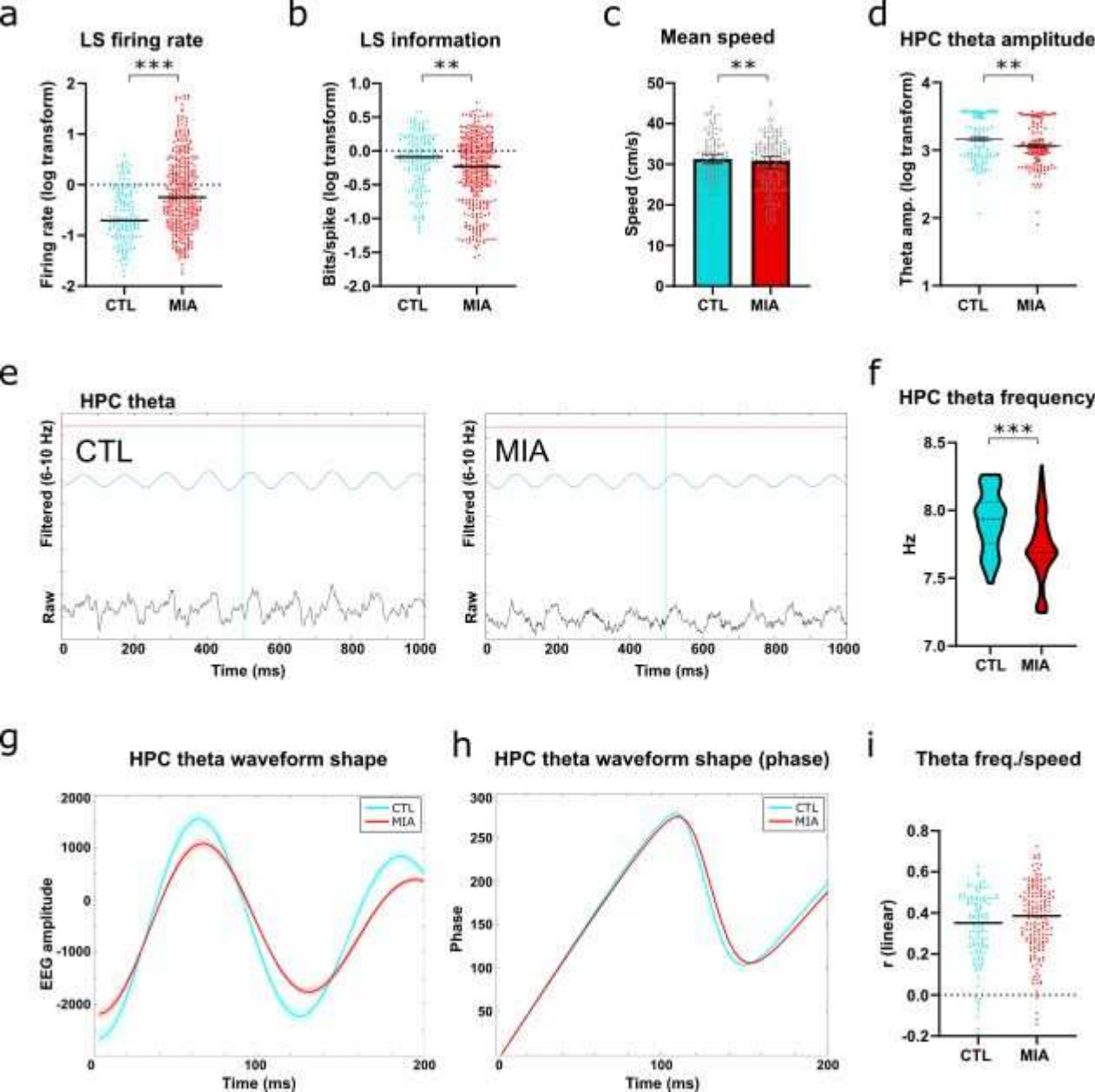
a
LS firing rate
***
Firing rate (log transform)
2
1
0
-1
-2
CTL
MIA
b
LS information
**
Bits/spike (log transform)
1.0
0.5
0.0
-0.5
-1.0
-1.5
-2.0
CTL
MIA
c
Mean speed
**
Speed (cm/s)
50
40
30
20
10
0
CTL
MIA
d
HPC theta amplitude
**
Theta amp. (log transform)
4
3
2
1
CTL
MIA
e
HPC theta
CTL
Filtered (6-10 Hz)
Raw
0
200
400
600
800
1000
Time (ms)
MIA
Filtered (6-10 Hz)
Raw
0
200
400
600
800
1000
Time (ms)
f
HPC theta frequency
***
Hz
8.5
8.0
7.5
7.0
CTL
MIA
g
HPC theta waveform shape
CTL
MIA
EEG amplitude
2000
1000
0
-1000
-2000
0
100
200
Time (ms)
h
HPC theta waveform shape (phase)
CTL
MIA
Phase
300
250
200
150
100
50
0
100
200
Time (ms)
i
Theta freq./speed
r (linear)
0.8
0.6
0.4
0.2
0.0
-0.2
CTL
MIA

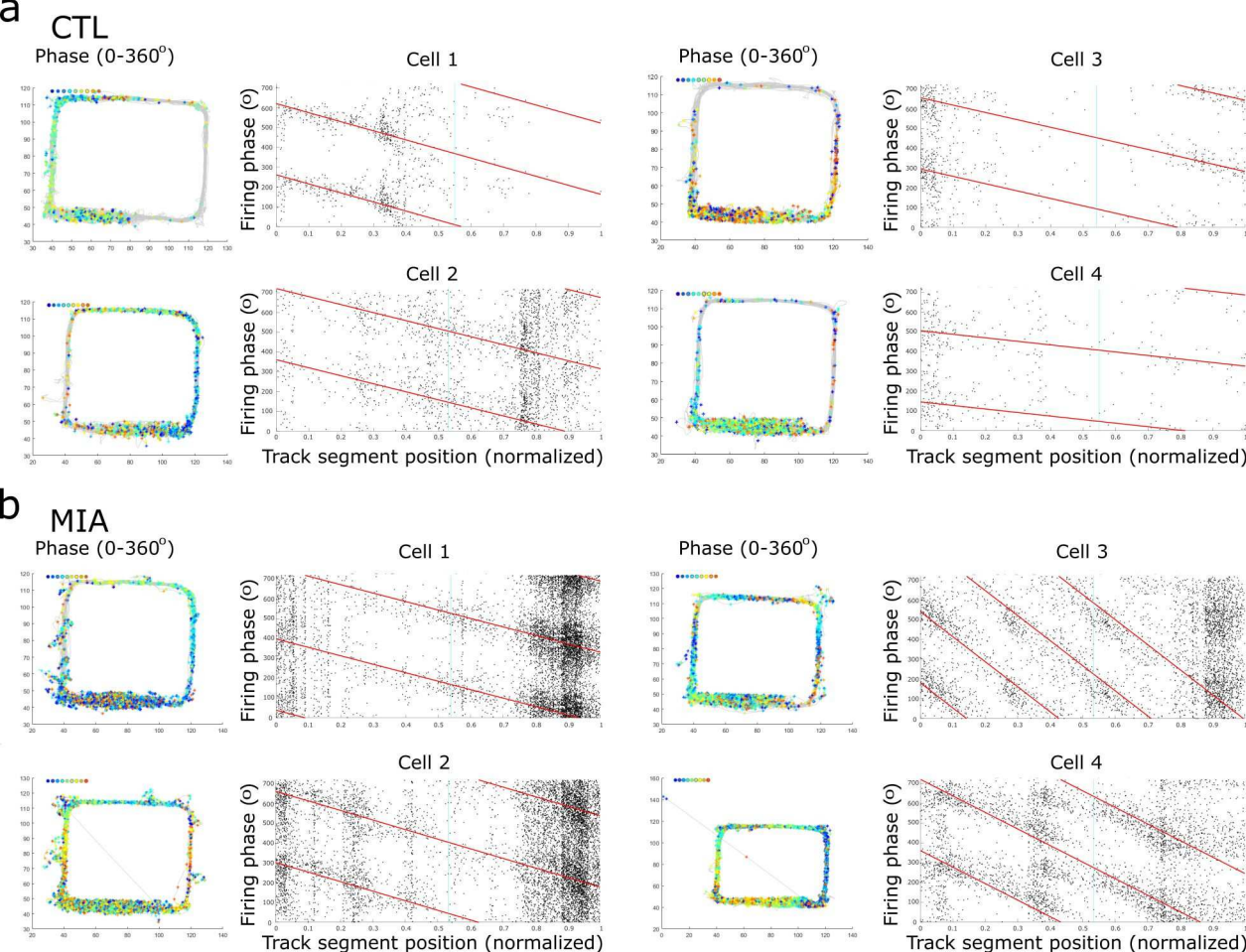
a
CTL
Phase (0-360°)
Cell 1
Cell 2
Cell 3
Cell 4
Firing phase (°)
Track segment position (normalized)
b
MIA
Phase (0-360°)
Cell 1
Cell 2
Cell 3
Cell 4
Firing phase (°)
Track segment position (normalized)

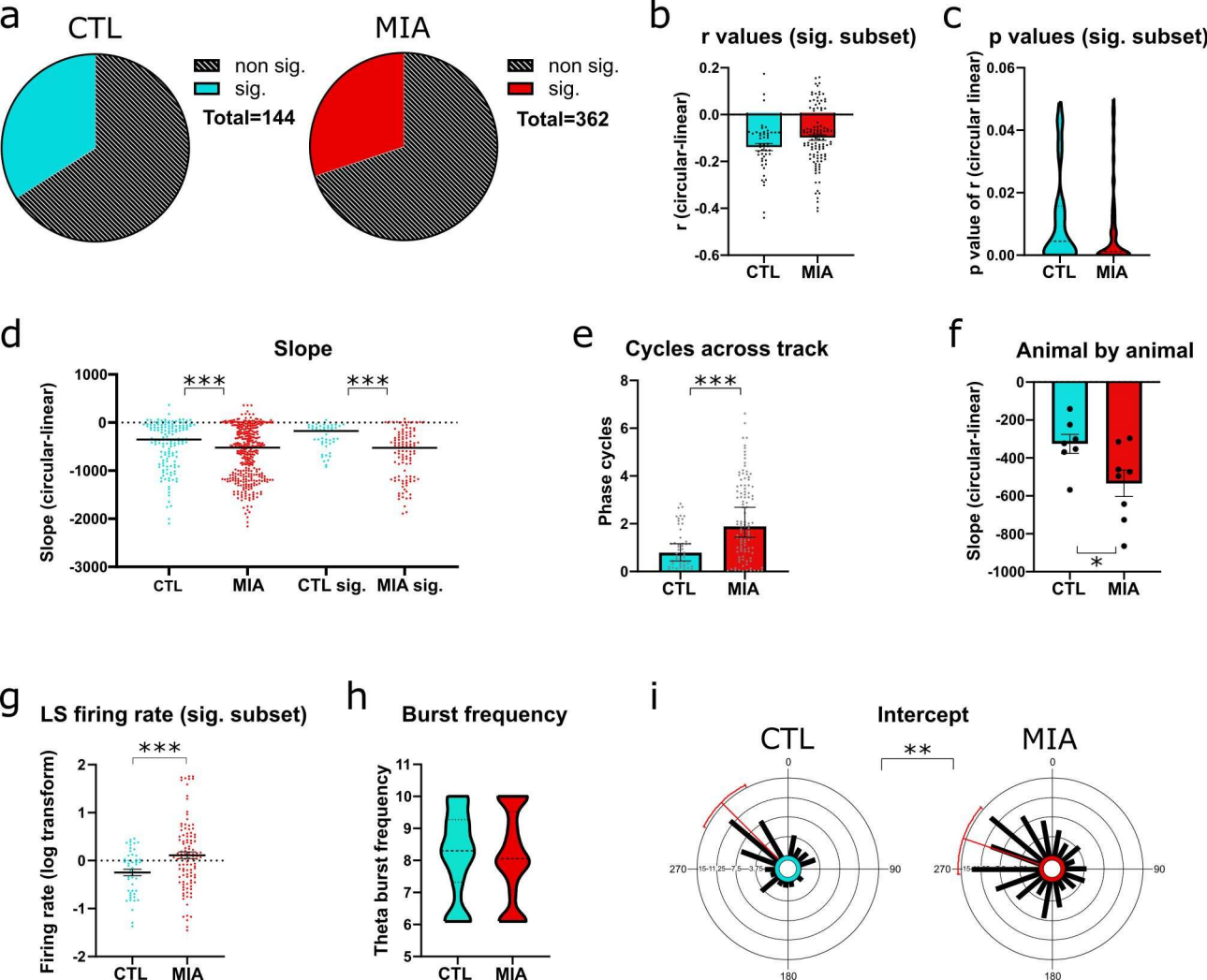
a
CTL
non sig.
sig.
Total=144
MIA
non sig.
sig.
Total=362
b
r values (sig. subset)
r (circular-linear)
0.2
0.0
-0.2
-0.4
-0.6
CTL
MIA
c
p values (sig. subset)
p value of r (circular linear)
0.06
0.04
0.02
0.00
CTL
MIA
d
Slope
Slope (circular-linear)
1000
0
-1000
-2000
-3000
***
***
CTL
MIA
CTL sig.
MIA sig.
e
Cycles across track
Phase cycles
8
6
4
2
0
***
CTL
MIA
f
Animal by animal
Slope (circular-linear)
0
-200
-400
-600
-800
-1000
*
CTL
MIA
g
LS firing rate (sig. subset)
Firing rate (log transform)
2
1
0
-1
-2
***
CTL
MIA
h
Burst frequency
Theta burst frequency
11
10
9
8
7
6
5
CTL
MIA
i
Intercept
CTL
**
MIA
0
90
180
270
0
90
180
270

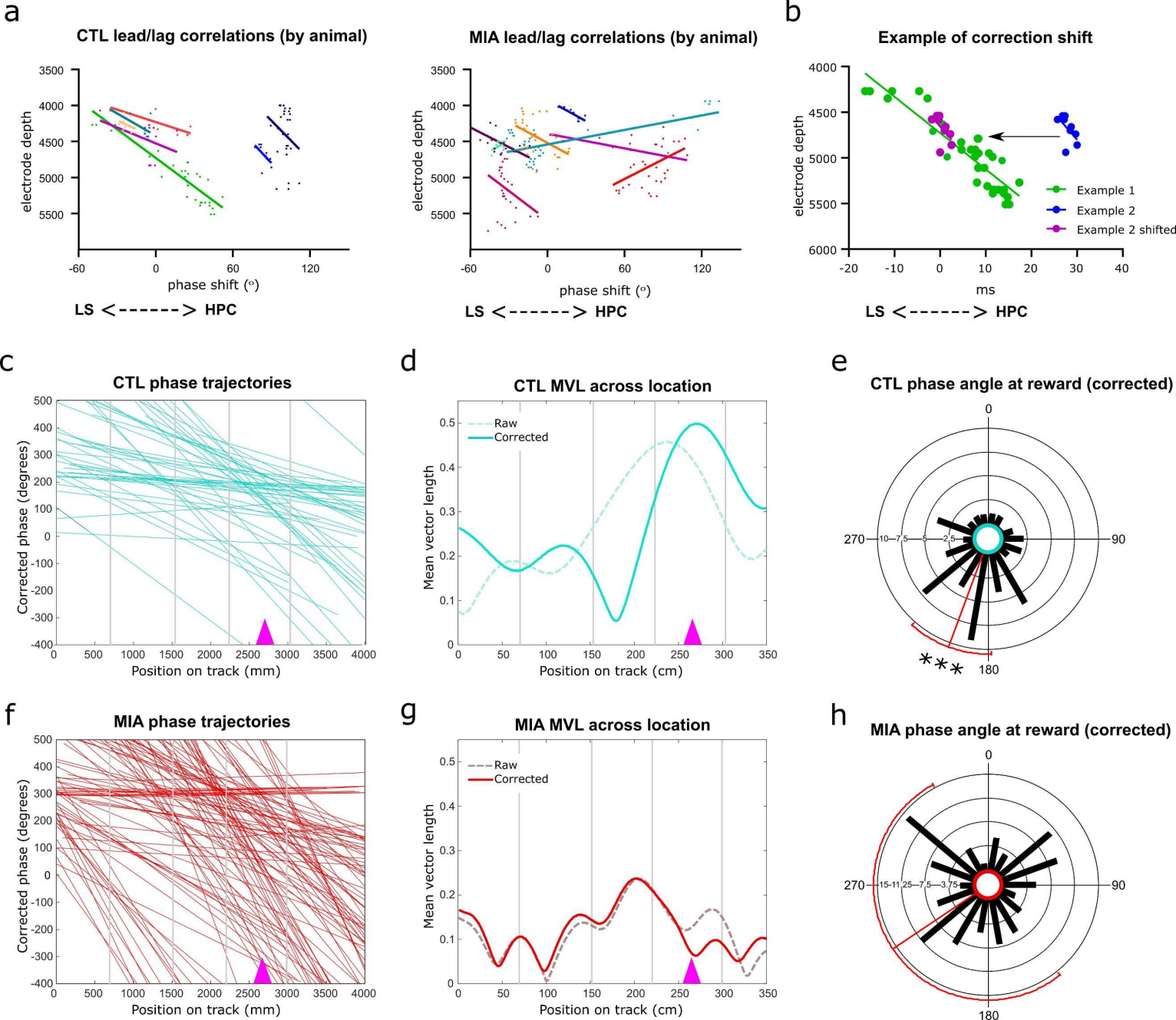
a
CTL lead/lag correlations (by animal)
MIA lead/lag correlations (by animal)
electrode depth
phase shift (°)
LS <------> HPC
b
Example of correction shift
electrode depth
ms
Example 1
Example 2
Example 2 shifted
LS <------> HPC
c
CTL phase trajectories
Corrected phase (degrees)
Position on track (mm)
d
CTL MVL across location
Raw
Corrected
Mean vector length
Position on track (cm)
e
CTL phase angle at reward (corrected)
***
f
MIA phase trajectories
Corrected phase (degrees)
Position on track (mm)
g
MIA MVL across location
Raw
Corrected
Mean vector length
Position on track (cm)
h
MIA phase angle at reward (corrected)

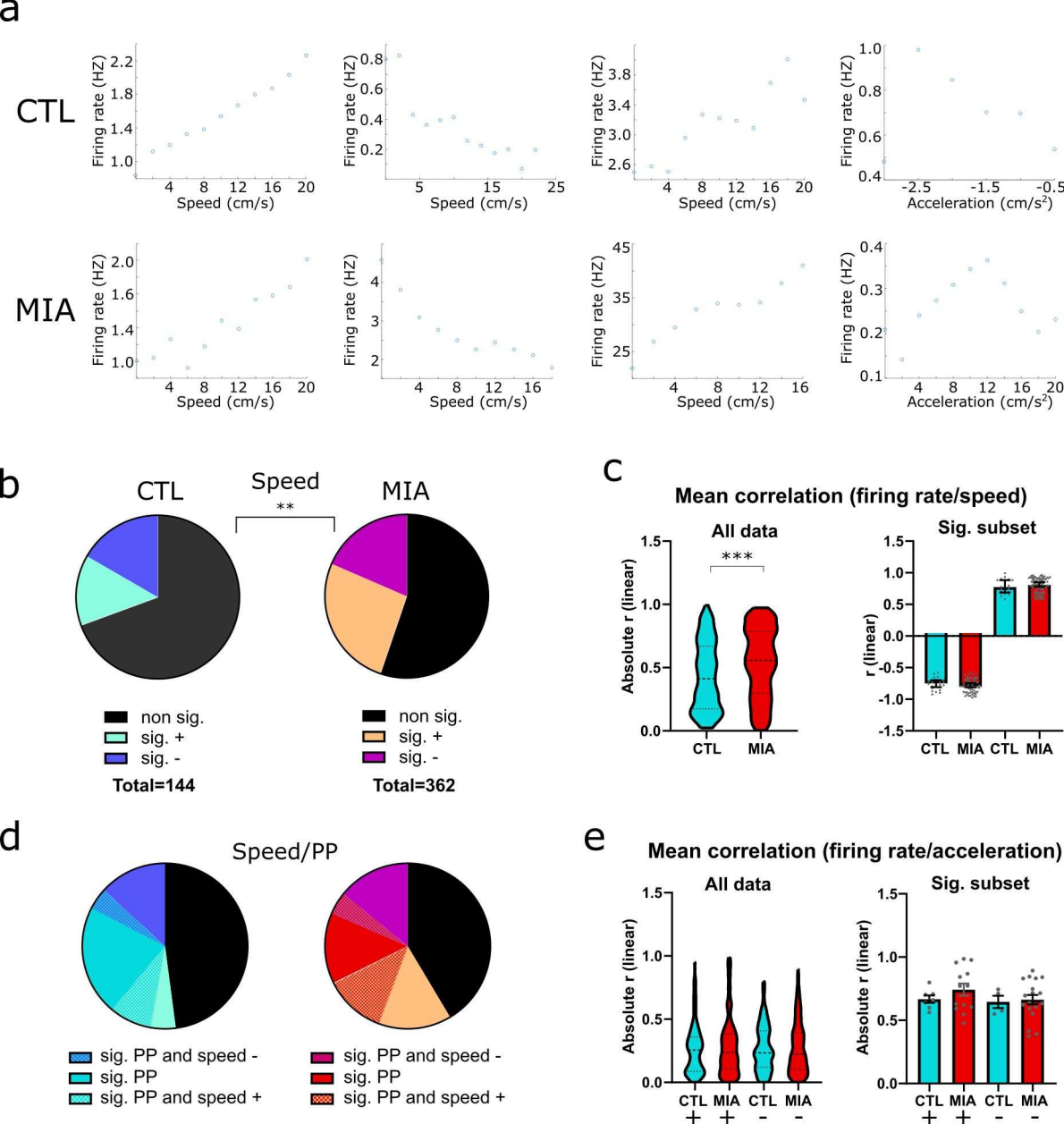
a
CTL
MIA
Firing rate (HZ)
Speed (cm/s)
Acceleration (cm/s²)
b
CTL
Speed
MIA
**
non sig.
sig. +
sig. -
Total=144
Total=362
c
Mean correlation (firing rate/speed)
All data
Sig. subset
***
Absolute r (linear)
r (linear)
CTL
MIA
d
Speed/PP
sig. PP and speed -
sig. PP
sig. PP and speed +
e
Mean correlation (firing rate/acceleration)
All data
Sig. subset
Absolute r (linear)
+
-

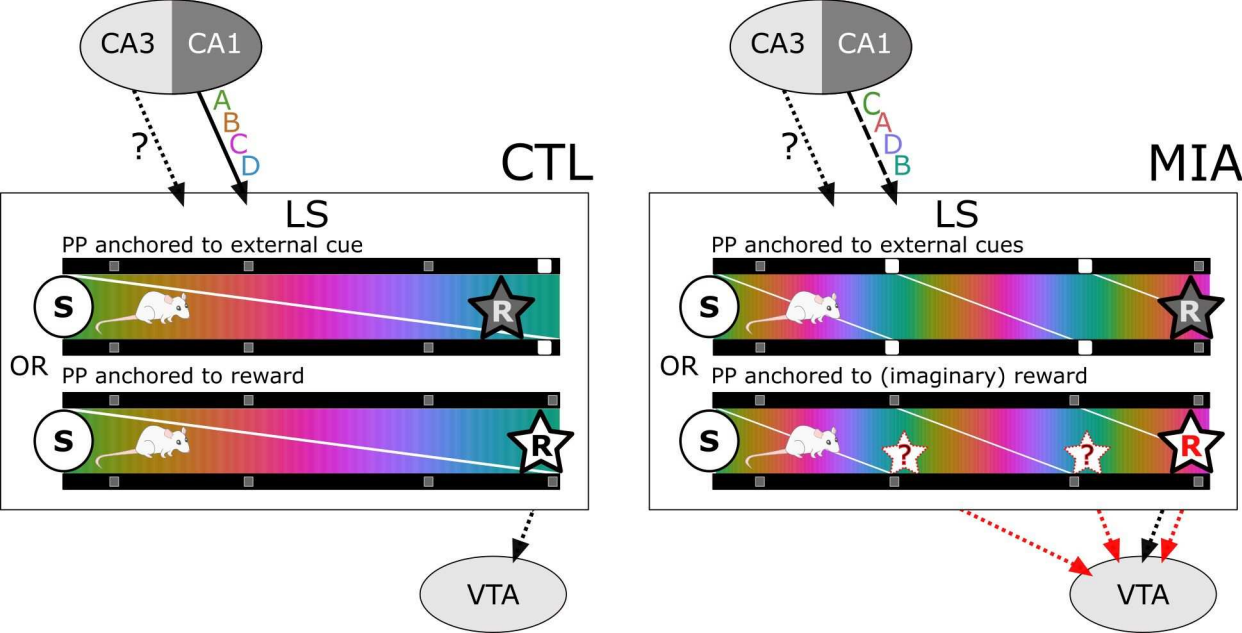
CA3
CA1
?
A
B
C
D
CTL
LS
PP anchored to external cue
S
R
OR
PP anchored to reward
S
R
VTA
CA3
CA1
?
C
A
D
B
MIA
LS
PP anchored to external cues
S
R
OR
PP anchored to (imaginary) reward
S
?
?
R
VTA